iScience

Article

Injured tubular epithelia-derived CCN1 promotes the mobilization of fibroblasts toward injury sites after kidney injury

Graphical abstract

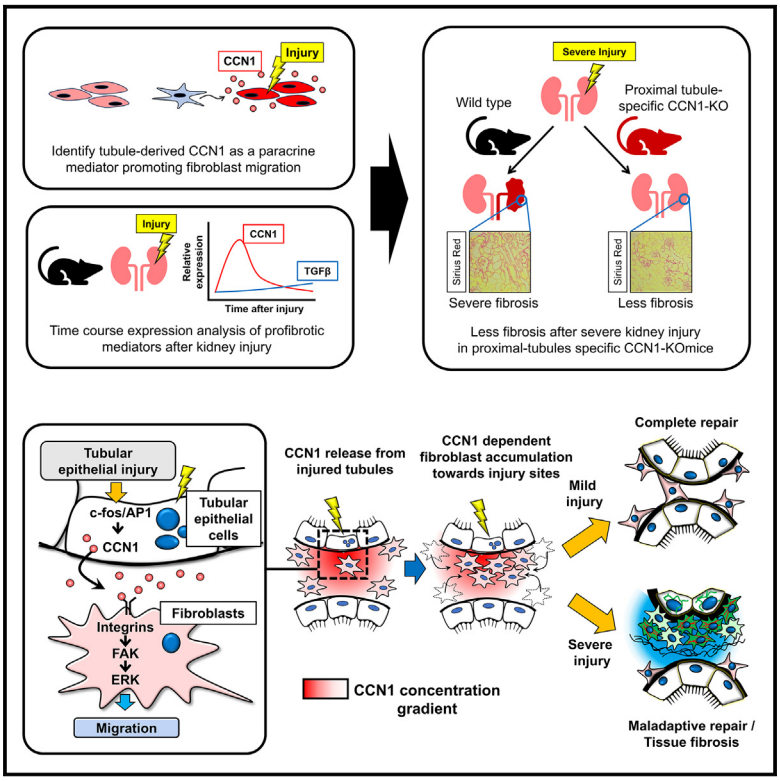

Highlights

- Injured tubular epithelia secrete CCN1 following acute kidney injury
- CCN1 promotes fibroblast chemotaxis through FAK-ERK signaling
- CCN1-KO in tubular epithelia reduces fibroblast accumulation at injury sites
- CCN1-KO in tubular epithelia ameliorates tissue fibrosis after severe kidney injury

Authors

Tomohiro Nakata, Yuhei Kirita, Minato Umehara, ..., Benjamin D. Humphreys, Satoaki Matoba, Tetsuro Kusaba

Correspondence

kusaba@koto.kpu-m.ac.jp

In brief

Biochemical mechanism; Molecular interaction; Integrative aspects of cell biology; Biology of human development

Nakata et al., 2025, iScience *28*, 112176
April 18, 2025 © 2025 The Author(s). Published by Elsevier Inc.
https://doi.org/10.1016/j.isci.2025.112176

CellPress

iScience

CellPress
OPEN ACCESS

Article

Injured tubular epithelia-derived CCN1 promotes the mobilization of fibroblasts toward injury sites after kidney injury

Tomohiro Nakata,[1] Yuhei Kirita,[1] Minato Umehara,[1] Masashi Nakamura,[1] Shinji Sawai,[1] Atsushi Minamida,[1] Hiroko Yamauchi-Sawada,[1] Yasuto Sunahara,[1] Yayoi Matoba,[1] Natsuko Okuno-Ozeki,[1] Itaru Nakamura,[1] Kunihiro Nakai,[1] Aya Yagi-Tomita,[1] Noriyuki Yamashita,[1] Keiichi Tamagaki,[1] Benjamin D. Humphreys,[2] Satoaki Matoba,[3] and Tetsuro Kusaba[1,4,*]

[1]Department of Nephrolog, Graduate School of Medical Science, Kyoto Prefectural University of Medicine, Kyoto, Japan
[2]Division of Nephrology, Washington University School of Medicine in St. Louis, St. Louis, MO, USA
[3]Department of Cardiovascular Medicine, Graduate School of Medical Science, Kyoto Prefectural University of Medicine, Kyoto, Japan
[4]Lead contact
*Correspondence: kusaba@koto.kpu-m.ac.jp
https://doi.org/10.1016/j.isci.2025.112176

SUMMARY

Humoral factors that prompt fibroblasts to migrate to an injury site at an appropriate time point are deemed indispensable for repair after kidney injury. We herein demonstrated the pivotal roles of injured tubule-derived cellular communication network factor 1 (CCN1) in the mobilization of fibroblasts to the injury site after kidney injury. Based on analyses of ligand-receptor interactions *in vitro* and tubular epithelial-specific transcriptomics *in vivo*, we identified the up-regulation of CCN1 during the early phases of kidney injury. CCN1 promotes fibroblast chemotaxis through focal adhesion kinase-extracellular signal-regulated kinase (ERK) signaling. *In vivo* analyses utilizing tubular-specific CCN1 knockout (KO) mice demonstrated the sparse accumulation of fibroblasts around injured sites after injury, resulting in ameliorated tissue fibrosis in CCN1-KO mice. These results reveal an epithelial-fibroblast CCN1 signaling axis that mobilizes fibroblasts to injured tubule early after acute injury but that promotes interstitial fibrosis at late time points.

INTRODUCTION

Recent epidemiological and experimental findings have shown that maladaptive tubular epithelial repair after acute kidney injury (AKI) drives the development of future tissue fibrosis.[1–3] Injured tubular epithelia release various pro-fibrotic humoral mediators that accelerate the differentiation of resident pericytes and fibroblasts to myofibroblasts and the production of the extracellular matrix (ECM), ultimately resulting in tissue fibrosis.[4–7] However, fibrosis is an adaptive phenomenon in the post-injury repair process, and the healing of injured tissue requires a highly plastic interstitium in which fibroblasts, macrophages, and vascular cells migrate, thereby forming scar tissue.[8,9] For example, the aggregation of fibroblast injury site is essential for tissue repair in skin[10,11] and cardiac tissue.[8,10,12–14] In the kidney fields, several reports showed the preventative role of fibroblasts on the fibrosis progression after injury.[15–17] Based on these findings, the early mobilization of fibroblasts to injury sites may be critical for adaptive or maladaptive tissue repair.

Humoral factors secreted by injured tubules are thought to induce the migration of fibroblasts to the site of injury and activate fibrotic signaling. During severe renal injury, the tubular epithelium undergoes cell-cycle arrest and secretes numerous pro-inflammatory and profibrotic mediators, such as transforming growth factor β (TGF-β), connective Tissue Growth Factor (CTGF), Wnt, hedgehog (Hh), and platelet-derived growth factor (PDGF), which induce tissue inflammation and fibrosis.[4,5,7,18–20] However, since these humoral factors are up-regulated in renal tissues in the subacute to chronic phase after injury, the mechanisms by which they act on ''fibroblasts'' in the acute phase and guide them to the site of injury remain unclear.

In the present study, we comprehensively analyzed the transcriptome in renal tubular epithelial cells and renal fibroblasts and identified cellular communication network factor 1 (CCN1) as a candidate injured tubular epithelia-derived matricellular protein. CCN1 has been shown to bind to integrins and play a role in cell migration and proliferation.[21] In the kidney, CCN1 was up-regulated early after injury,[22,23] and neutralizing antibodies reduced renal fibrosis[24,25]; however, its roles in renal injury and the repair process have not yet been elucidated in detail. In the present study, we investigated the relationship between tubular epithelial cells and surrounding fibroblasts, with a focus on CCN1 and its ability to migrate to the site of injury.

This is an open access article under the CC BY-NC license (http://creativecommons.org/licenses/by-nc/4.0/).

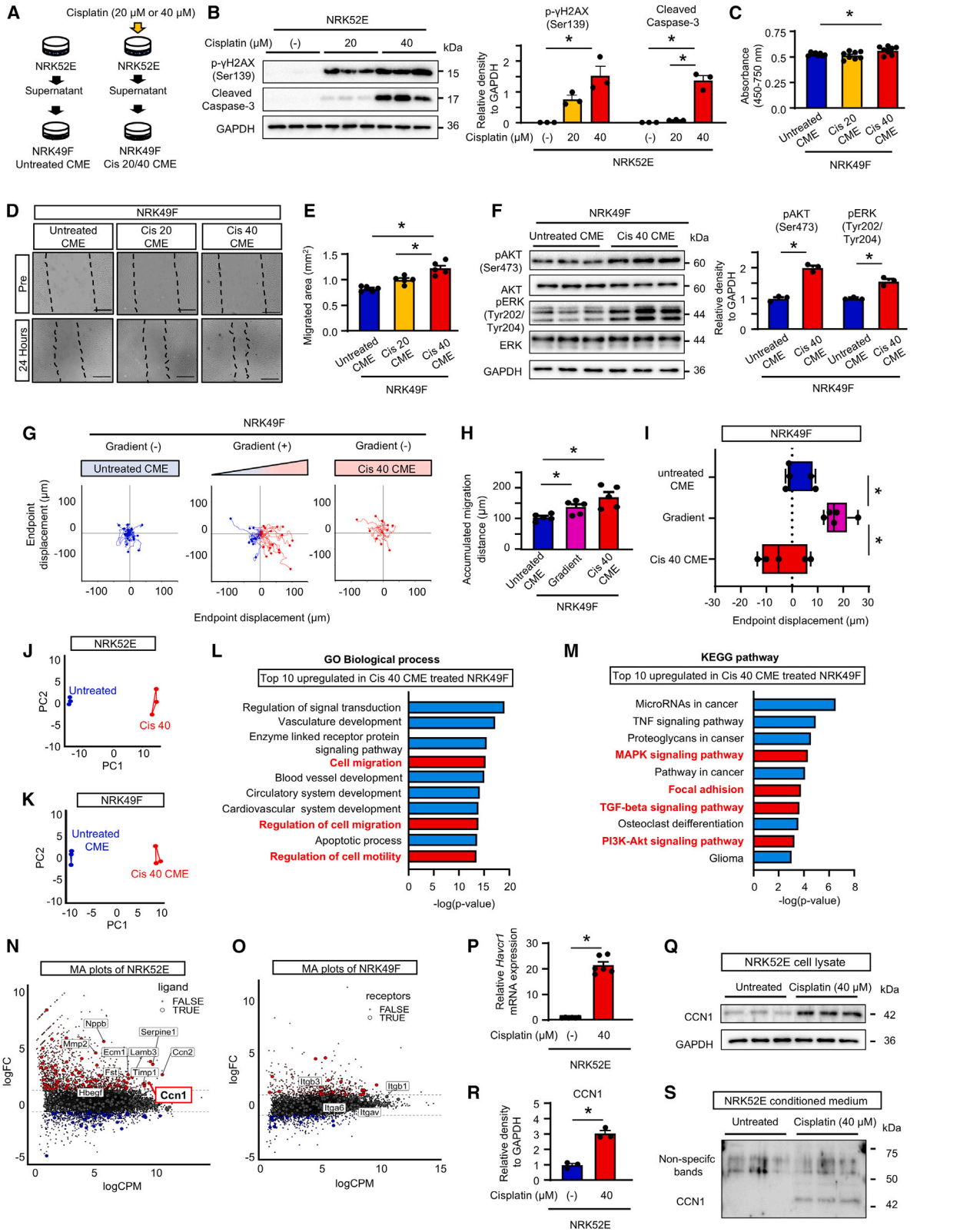

(legend on next page)

RESULTS

Cultured media of injured tubular epithelia accelerates fibroblast migration

To examine the paracrine effects of epithelial cells on fibroblasts, we performed *in vitro* experiments using cultured media (CM) from NRK52E and NRK49F (CME and CMF, respectively, Figure 1A). Compared with CMF, CME accelerated NRK49F proliferation and migration (Figure S1). We next obtained CM from injured tubular epithelia on fibroblasts. Cisplatin up-regulated γH2AX phosphorylation and cleaved caspase-3 activation in NRK52E (Figure 1B). CM from 40 μM of cisplatin-treated NRK52E (Cis 40-CME) increased the proliferation of NRK49F (Figure 1C). The scratch assay demonstrated that NRK49F migration was accelerated more by Cis 40-CME than by untreated CME (Figures 1D and 1E) and showed chemotaxis toward Cis 40-CME (Figures 1G–1I). Regarding the migration and proliferation-related molecules, Cis 40-CME increased in the phosphorylation of AKT and ERK (Figure 1F). Regarding the effect of the severity of tubular injury on CME (Cis 20-CM vs. Cis 40-CM, Figure 1B), fibroblast migration was accelerated more by Cis 40-CME than by Cis 20-CME, whereas no significant differences were observed in proliferation or chemotaxis (Figures 2C–2E and S2A–S2C). Overall, CME from injured tubular epithelia accelerated the proliferation and migration of fibroblasts in general and directed migration of fibroblasts to more injured tubular epithelia.

Comparisons of transcriptomics of tubular epithelia and CM-treated fibroblasts identify CCN1 as a candidate marker for fibroblast migration

We next examined differences in the transcriptome between NRK52E treated with 40 μM of cisplatin or vehicle by RNA sequencing (RNA-seq). We also compared the transcriptome between NRK49F treated with Cis 40-CME and untreated CME. Unsupervised analyses of gene expression by a principal component analysis revealed that the transcriptional landscapes of untreated and cisplatin-treated NRK52E and untreated CME-treated and Cis 40-CME-treated NRK49F were separated into independent clusters, indicating distinct gene expression patterns for each experimental group (Figures 1J and 1K). We annotated gene expression using the Gene Ontology biological process and found that terms related to cell migration were up-regulated in Cis 40-CME-treated NRK49F (Figures 1L and 1M). To identify the mediators secreted from injured epithelial cells responsible for this effect, we analyzed the gene expression patterns of ligands in cisplatin-treated NRK52E that act in a paracrine manner. Boiling CME for 1 h significantly attenuated the Cis 40-CME-mediated acceleration of NRK49F migration, suggesting that a protein/peptide was responsible[26] (Figure S3). Based on previous findings on the molecules up-regulated in the earlier phase after AKI and up-regulated receptors in Cis 40-CME-treated NRK49F, we identified *Ccn1* as a candidate (Figures 1N and 1O). We confirmed the up-regulation of the CCN1 protein in both cell lysates and CME from injured tubular epithelia in which *Havcr1* mRNA, a tubular injury marker, was increased after cisplatin treatment (Figures 1P–1S).

CCN1 up-regulation in injured proximal tubules *in vivo*

To examine the up-regulation of CCN1 in injured proximal tubules (PTs), we used bigenic mice with a PT-specific tamoxifen-inducible Cre (SLC34a1GCE) and the tdTomato reporter (R26tdTomato).[27] After exclusively labeling PTs, 15 mg/kg of cisplatin was injected into mice (Figure 2A). Blood urea nitrogen (BUN) was increased by the cisplatin injection (Figure 2B), and

Figure 1. Injured tubular epithelia-derived culture media increases the proliferation and chemokinesis of fibroblasts, and transcriptomics identified CCN1 as a candidate

(A) Experimental scheme. Cultured media was obtained from untreated, or 20 and 40 μM of cisplatin-treated NRK52E (untreated CME, Cis 20-CME, Cis 40-CME, respectively).

(B) Western blot of protein lysates from NRK52E for DNA damage and apoptosis markers. The optical density of γH2AX and cleaved caspase-3 bands was normalized against GAPDH. $n = 3$ each.

(C) Cell proliferation analysis of NRK49F treated with untreated, 20 Cis-CME or 40 Cis-CME. $n = 8$ each.

(D) Representative pictures of the scratch migration assay of CME-treated NRK49F. The scale bars indicate 500 μm.

(E) Quantification of the migrated area of NRK49F. $n = 5$ each.

(F) Western blot analysis of pAKT, AKT, pERK, ERK, and GAPDH in NRK49F. The optical densities of the pAKT and pERK bands were normalized against GAPDH. $n = 3$ each.

(G) Representative pictures of polar plots displaying the trajectories of NRK49F migrating in untreated CME (left), in Cis 40-CME (right), and in gradients in between (middle). The gradient is formed from untreated CM on the left side to Cis 40-CME on the right side of the plots.

(H) Analysis of NRK49F migration by the average track diameter. $n = 5$ each compartment.

(I) Analysis of average endpoint displacements indicating chemotaxis in response to Cis 40-CME. $n = 5$ each compartment.

(J) Principal component analysis (PCA) clustering with samples from cisplatin-treated or untreated NRK52E demonstrated clear divergence.

(K) PCA clustering with samples from NRK49F treated with untreated CME or Cis 40-CME demonstrated clear divergence.

(L and M) Exhibited the Gene Ontology (GO) analysis of significant differentially expressed genes in NRK49F treated with untreated CME or Cis 40-CME (top 10 up-regulated GO terms of biological processes (L) and KEGG pathways (M)).

(N) MA plot showing a comparison of 40 μM of cisplatin-treated and vehicle-treated NRK52E.

(O and P) MA plot showing a comparison of NRK49F treated with untreated CME or Cis 40-CME (P) qPCR analysis of *Havcr1* from the RNA of the cisplatin-treated NRK52E lysate. $n = 6$ each.

(Q) Western blot analysis of CCN1 in the 40 μM of cisplatin-treated NRK52E lysate. $n = 3$ each.

(R) The optical density of CCN1 was normalized against GAPDH. $n = 3$ each.

(S) Western blot analysis of CCN1 in untreated CME or Cis 40-CME. All scratch migration assays or single-cell migration assays were performed after mitomycin pretreatment. $n = 3$ each.

For all groups, data are means ± SEM. Endpoint displacements in (I) are reported in a box and whisker plot. Statistical analyses were performed by unpaired t test for comparisons of two variables and by ANOVA and Dunnett's post hoc test for comparisons of multiple variables. $^*p < 0.05$.

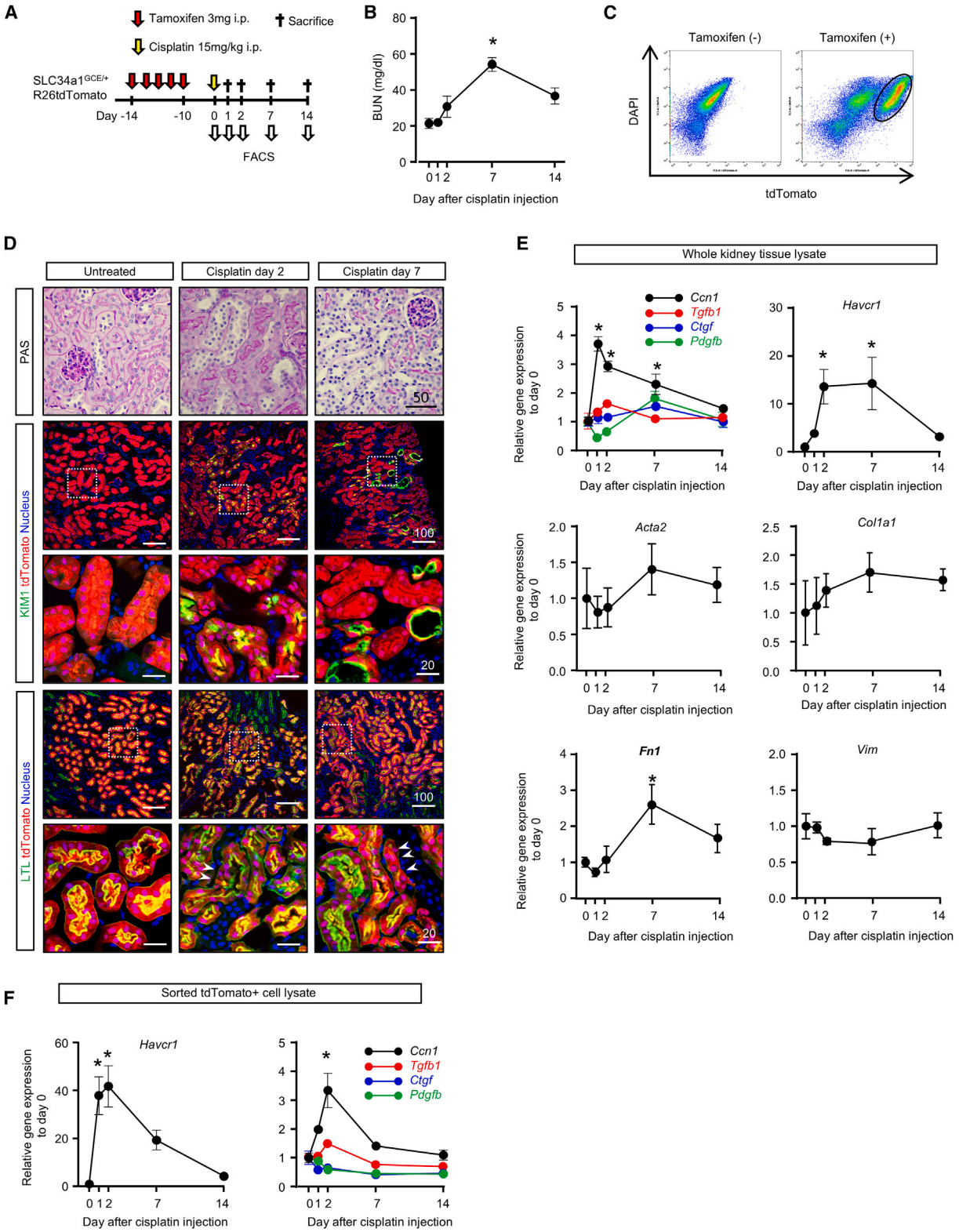

Figure 2. PT-specific transcriptomics reveal *Ccn1* up-regulation in the early phase after cisplatin-induced kidney injury *in vivo*

(A) Experimental scheme. Bigenic mice (SLC34a1GCE × R26tdTomato) received intraperitoneal injections of cisplatin (15 mg/kg) and tamoxifen (3 mg/kg at each time point) as indicated.

(legend continued on next page)

tdTomato+ tubular epithelia were collected by fluorescence-activated cell sorting (FACS) (Figures 2A and 2C). PAS staining showed extensive tubular injury, and immunofluorescence staining revealed positive staining of KIM1, a tubular injury marker, and reduced staining of LTL, a tubular integrity marker, in tdTomato+ cells (Figure 2D). A qPCR analysis of RNA from isolated tdTomato+ epithelia and whole kidney tissue revealed that the expression of *Ccn1* and *Havcr1* was significantly up-regulated after injury, whereas the expression of other profibrotic genes, namely, *Tgfb1*, *Ctgf*, and *Pdgfb*, did not change after the cisplatin injection (Figures 2E and 2F). To generalize the up-regulation of CCN1 after injury, we further analyzed its expression in various kidney injury models (Figure S4A). In the ischemia-reperfusion injury (IRI) model, *Ccn1* expression was up-regulated 3 days after injury in a manner that was dependent on the severity of injury (Figures S4B and S4C). In the aristolochic acid injury model, qPCR demonstrated that *Ccn1*, tubular injury markers, and fibrosis-related mediators were up-regulated 14 days after injury (Figures S4D and S4E). In the unilateral ureteral ligation model, *Ccn1* was up-regulated after surgery and gradually decreased thereafter, whereas the markers of other profibrotic mediators (*Ctgf*, *Tgfb1*, and *Pdgfb*), myofibroblasts (*Acta2*), and ECM (*Fn1*, *Col1a1*) gradually increased (Figures S4F–S4H). We also analyzed *CCN1* expression using the publicly available transcriptomics database of the human kidney (Figure S5). Bulk RNA-seq of a whole transplanted kidney revealed that the transient up-regulation of *CCN1* occurred just after kidney transplant, a condition that simulates IRI in the human kidney (Figure S5A).[28] Single-cell-based transcriptomics of healthy, chronic kidney disease (CKD), and AKI human kidneys indicated the up-regulation of *CCN1* in PTs of the AKI kidney (Figures S5B and S5C).[29] While the expression of *CCN1* was also observed in healthy and CKD kidneys, *CCN1* correlated with the expression of *HAVCR1*, indicating that subclinically injured PTs expressed *CCN1* even in heathy human kidneys (p = 0.013, R^2 = 0.14, Figure S5D). Overall, the up-regulation of CCN1 after injury was observed in multiple independent AKI models and in humans, and the dynamics of its expression were distinct from other well-known profibrotic factors released from injured tubular epithelia.

CCN1 activates FAK signaling and accelerates fibroblast migration

We next examined the effects of human recombinant CCN1 on fibroblasts. Recombinant CCN1 increased the proliferation of NHDF, a human fibroblast cell line (Figure 3A), and migration (Figures 3C and 3D), whereas it did not affect alpha-smooth muscle actin (αSMA) expression (Figure 3B). A gradient of CCN1 (0–2 μg/mL) significantly increased chemotaxis in NHDF (Figures 3E–3G). Based on its local interaction with integrins, a receptor of CCN1, we focused on the focal adhesion kinase (FAK) pathway. Western blotting revealed that the phosphorylation of FAK (pFAK) and its downstream molecules (pERK, pAKT) was increased by CCN1 in NHDF (Figure 3H). Immunofluorescence analyses revealed the up-regulation of pFAK in CCN1 treated-NHDF (Figure 3I). Western blotting and immunofluorescence analyses revealed that the pFAK also increased in Cis 40-CME-treated NRK49F (Figures 3I and 3J). Immunofluorescence analysis revealed that the number of pFAK+ cells increased around the KIM1+ injured tubules after cisplatin injection *in vivo*, and bulk of pFAK+ cells were positive for PDFGRβ, indicating that fibroblasts accumulated at the injury site (Figure 3K). Similar findings were observed in the mice that received IRI (Figure 3L).

Genetic deletion of Ccn1 in tubular epithelial cells reduces the accumulation of fibroblasts around damaged tubular epithelia and subsequent tissue fibrosis after severe injury

We next examined whether CCN1 regulates fibroblast migration and contributes tissue fibrosis after injury *in vivo* by generating a tubule-specific knockout (KO) of CCN1 in AKI using mice (hereafter referred to as CCN1-KO for homozygous mutant mice). To directly confirm the deletion of CCN1 in PTs, we generated trigenic mice with a SLC34a1GCE allele, a R26tdTomato allele with or without CCN1-KO. After the exclusive labeling of PTs, mice were sacrificed 2 days after the cisplatin injection (Figure 4A). Immunofluorescence analysis demonstrated that PTs were labeled with tdTomato in both CCN1-KO and wild-type (WT) mice, and KIM1 expression was detected in both injured kidneys (Figure 4B). Reverse-transcription PCR (RT-PCR) on sorted tdTomato+ tubular epithelial cells demonstrated the loss of *Ccn1* gene expression in CCN1-KO mice (Figure 4C).

We next analyzed the effect of PT-specific deletion of CCN1 on uninjured kidneys (Figure S6A). There was no difference in BUN and renal histology between CCN1-KO and WT mice 10 days and 24 days after last tamoxifen injection (Figures S6B and S6C). qPCR analysis demonstrated that there were no significant differences in expressions of *Havcr1*, *Slc34a1*, *Lrp2*, *Tgfb1*, *Pdgfrb*, *Fn1*, and *Acta2* between WT and CCN1-KO mice (Figure S6D), suggesting that PT-specific loss of CCN1 function did not affect any morphological and functional changes at baseline.

We then analyzed the effect of PT-specific deletion of CCN1 on cisplatin nephrotoxicity. Serial measurements of BUN showed that BUN increased at 4 days after cisplatin injection and returned to baseline; there was no difference between WT and CCN1-KO mice (Figure 4D). We first checked the

(B) Changes in BUN after the administration of cisplatin. n = 4–5 per group.
(C) Isolation of tdTomato+ tubular epithelial cells using FACS.
(D) Histological analysis of the kidney after the cisplatin injection. PAS staining of kidney sections and immunostaining of LTL and KIM1. The scale bars indicate 50 μm in PAS staining, 100 μm in low-power field pictures and 20 μm in high-power field pictures in immunostaining.
(E) Time-course analyses of qPCR of RNA from the whole kidney for the representative markers of tubular injury (*Havcr1*), profibrotic factors (*Ccn1*, *Tgfb1*, *Ctgf*, and *Pdgfb*), myofibroblast (*Acta2*), mesenchymal cell (*Vim*), and extracellular matrix (*Col1a1* and *Fn1*). n = 4–5 per group.
(F) Time-course analyses of qPCR of RNA from the isolated tdTomato+ tubular epithelial cells. n = 4–5 per group.
For all groups, data are means ± SEM. Statistical analyses were performed by unpaired t test for comparisons to day 0 (B, E, F). *p < 0.05 vs. day 0.

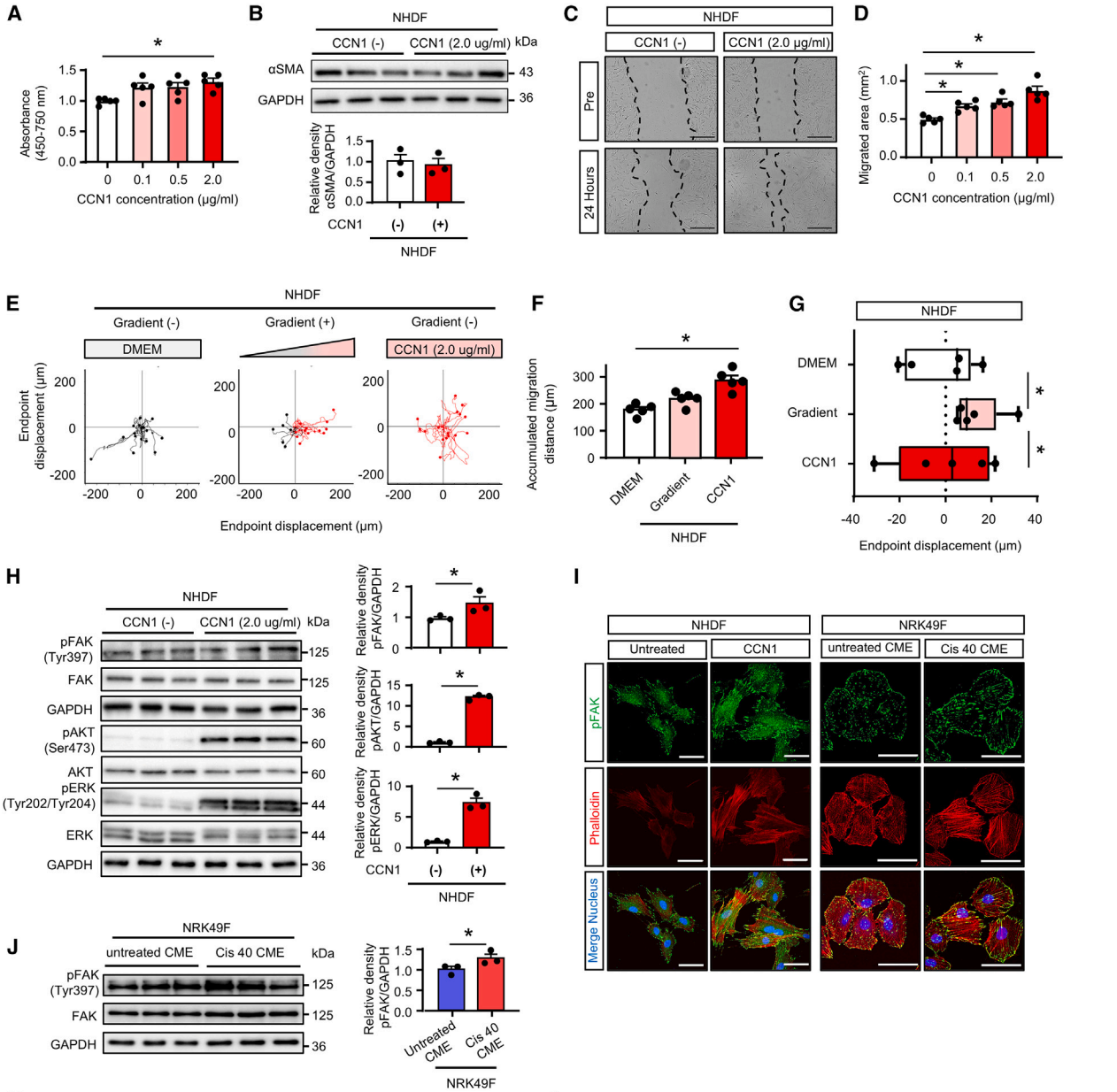

(legend on next page)

phenotypes 4 days after cisplatin injection when its nephrotoxicity became histologically evident in PAS staining and γH2AX immunostaining (Figures S7A and S7B). Immunofluorescence analysis revealed that γH2AX+ tubular epithelial cells were found in both CCN1-KO and WT mice treated with cisplatin and that PDGFRβ+ interstitial fibroblasts cells accumulated around tubules containing γH2AX+ cells in WT mice, but not in CCN1-KO mice (Figure 4E). pFAK+ cells accumulated around KIM1+ injured tubules only in WT mice, not in CCN1-KO mice, and bulk of interstitial pFAK+ cells were positive for PDGFRβ (Figure 4E). qPCR analysis demonstrated that there were no significant differences in expressions of *Havcr1*, *Tgfb1*, *Pdgfrb*, and *Acta2* between WT and CCN1-KO mice; however, *Vim* was slightly increased and *Slc34a1* was slight decreased in CCN1-KO mice (Figure S7C). At 14 days after cisplatin injection, Sirius red staining showed mild interstitial fibrosis, but there was no difference between WT and CCN1-KO mice (Figures 4F and 4G). qPCR analysis demonstrated that there were no significant differences in gene expressions of the tubular injury, tubular integrity, macrophages, and fibrosis markers between WT and CCN1-KO mice (Figure 4H).

We further examined the effect of *Ccn1* deletion on the severe AKI model, 35 min unilateral IRI (Figure 5A). We confirmed the loss of *Ccn1* gene expression in CCN1-KO mice with IRI by RT-PCR on sorted tdTomato+ tubular epithelial cells (Figures 5B and 5C). We next checked the phenotypes 1 day after IRI and extensive tissue injury was evident in both WT and CCN1-KO mice in PAS staining (Figure S8A). Immunofluorescence analysis revealed that pFAK+ cells accumulated around KIM1+ injured tubules in WT mice, but not in CCN1-KO mice (Figure 5D). Bulk of accumulated interstitial pFAK+ cells were positive for PDGFRβ (Figure 5D). qPCR analysis demonstrated that there were no significant differences in expressions in tubular injury markers, integrity markers, and fibrosis-related markers between WT and CCN1-KO mice, but *Ccl2* and macrophage marker were rather increased in CCN1-KO mice at 1 day after injury (Figure S8B). At later time point of 14 days after IRI, Sirius red staining showed the extensive interstitial fibrosis in IRI kidneys, and it was significantly attenuated in CCN1-KO mice (Figures 5E and 5F). qPCR analysis at 14 days after injury demonstrated that gene expressions of the tubular injury markers (*Havcr1* and *Lcn2*), *Ccl2*, *Adgre*, and fibrosis markers (*Pdgfrb*, *Acta2*, *Col1a1*, *Fn1*, and *Tgfb1*) were significantly lower in IRI kidneys of CCN1-KO mice than those of WT mice (Figure 5G). Overall, PT-specific deletion of *Ccn1* reduced the accumulation of pFAK+ cells into the tissue injury site and ameliorated subsequent tissue fibrosis only after severe injury (35 min IRI), but not after mild injury (cisplatin nephrotoxicity).

Gene deletion of CCN1 reduced fibroblast migration by injured tubule-derived CM *in vitro*

To test the further mechanistic insights, we generated CCN1-KO NRK52E using CRISPR-Cas9-based gene editing. We targeted the gene-editing site to exon 2, which precedes sequences encoding integrin-binding sites (Figure 6A). We isolated single-cell colonies in which CCN1 expression was completely lost in both cell lysates and CME (Figures 6B and 6C). CM from cisplatin-treated CCN1-KO NRK52E (CCN1-KO Cis 40-CME) failed to increase the proliferation and migration of NRK49F compared to Cis 40 CME control (Figures 6D–6F). The chemotaxis and chemokinesis of NRK49F were observed between CME from cisplatin-treated NRK52E with or without CCN1-KO (Figures 6G–6I). In addition, increases in the chemotaxis and chemokinesis of NRK49F mediated by CM from cisplatin-treated NRK52E disappeared following the deletion of CCN1 in NRK52E (Figures 6J–6L). Western blotting revealed that the phosphorylation of ERK by Cis 40-CME was partially inhibited by the deletion of CCN1 in NRK52E (Figure 6M).

Inhibition of FAK reduced fibroblast migration by injured tubule-derived CM *in vitro*

To examine the role of CCN1-FAK signaling in NRK49F migration, we knocked down *Ptk2* (encoding FAK) in NRK49F by small interfering RNA (siRNA) transfection. qPCR and western blotting demonstrated that siRNA transfection down-regulated *Ptk2* mRNA and FAK protein expression (Figure 7A). This *Ptk2* knockdown indeed significantly reduced the Cis 40-CME-mediated acceleration of NRK49F migration, chemotaxis, and chemokinesis (Figures 7B–7F). Western blotting demonstrated that the Cis 40-CME-mediated phosphorylation of ERK and AKT in NRK49F was also attenuated by the knockdown of *Ptk2* (Figure 7G). Regarding the effects of the pharmacological inhibition of FAK

Figure 3. CCN1 increases the proliferation and chemokinesis of fibroblasts

(A) Cell proliferation assay data indicated that CCN1 accelerated NHDF proliferation. $n = 5$ each.

(B) Western blot of protein lysates from NHDF for αSMA. The optical densities of αSMA bands were normalized against GAPDH. $n = 3$ each.

(C) Representative pictures of the scratch migration assay of NHDF treated with CCN1. The scale bars indicate 500 μm.

(D) Quantification of the migrated area of NHDF. $n = 5$ each.

(E) Representative pictures of polar plots displaying the trajectories of NHDF migrating in DMEM (left), in DMEM with CCN1 (right), and in gradients in between (middle).

(F) Analysis of NHDF migration by the average track diameter. $n = 5$ each compartment.

(G) Analysis of average endpoint displacements indicating chemotaxis in response to CCN1. $n = 5$ each compartment.

(H) Western blot analysis of pAKT, AKT, pERK, ERK, and GAPDH in NHDF 30 min after treatments. Western blot analysis of pFAK, FAK, and GAPDH in NHDF 10 min after treatments. The optical densities of bands of these molecules were normalized against GAPDH. $n = 3$ each.

(I) Representative immunofluorescence images of pFAK and Phalloidin in NHDF treated with CCN1 and NRK49F with cisplatin-treated NRK52E-derived CM.

(J) Western blot analysis of pFAK, FAK, and GAPDH in NRK49F treated with untreated CME or Cis 40-CME for 10 min $n = 3$ each.

(K and L) Representative co-immunofluorescence images of KIM1-pFAK and PDGFRβ-pFAK at 4 days after cisplatin injection (K) and at 1 day after unilateral IRI (L). The scale bars indicate 50 μm in (I), 50 μm in low-power field pictures, and 20 μm in high-power field pictures in (K) and (L). All scratch migration assays or single-cell migration assays were performed after mitomycin pretreatment.

For all groups, data are means ± SEM. Endpoint displacements in (G) are reported in a box and whisker plot. Statistical analyses were performed by unpaired t test for comparisons of two variables and by ANOVA and Dunnett's post hoc test for comparisons of multiple variables. $^*p < 0.05$.

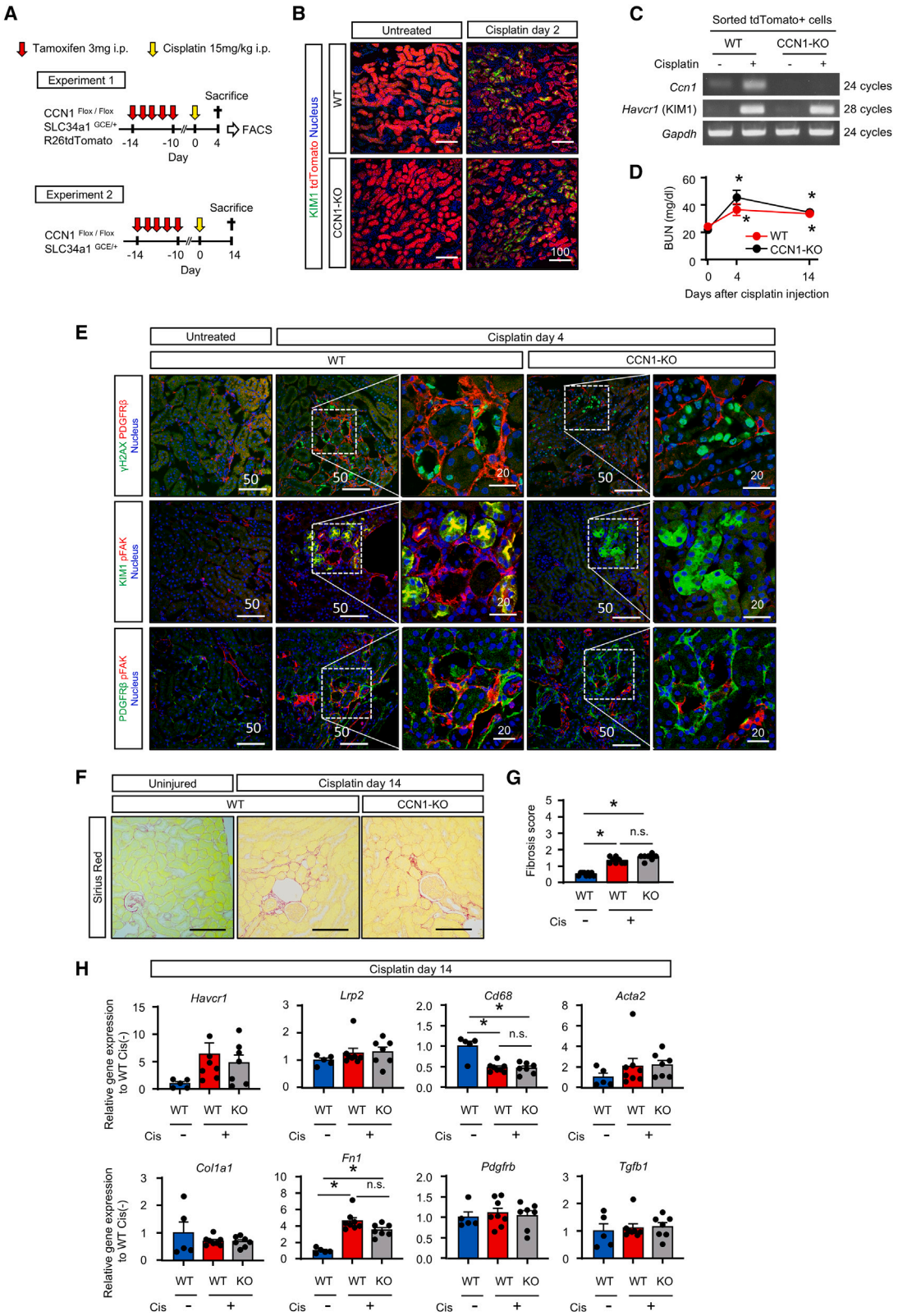

(legend on next page)

on CCN1 signaling, western blotting demonstrated that FAK inhibition reduced the CCN1-mediated phosphorylation of FAK, ERK, and AKT in NHDF. CCN1-mediated cell migration was also abrogated by the FAK inhibitor. In addition, we examined the effects of ERK inhibition on CCN1-mediated NHDF migration. Western blotting demonstrated that the CCN1-mediated phosphorylation of ERK (Figures S9A and S9B) and cell migration was inhibited by the ERK inhibitor (Figures S9C and S9D).

We lastly attempted to elucidate the regulatory mechanism of CCN1 in injured tubular epithelia. Based on previous findings showing the presence of two activator protein 1 (AP-1)-binding sites in the promoter of *CCN1*,[30] we performed a regulon analysis of RNA sequences. We identified 48 up-regulated transcriptional factors in cisplatin-treated NRK52E, including Jun (Figure S10A). We investigated the effect of pharmacological inhibition of c-fos/AP-1 by T5224 and found that this inhibited the cisplatin-induced up-regulation of *Ccn1* in NRK52E (Figure S10B).

DISCUSSION

Fibrogenic processes after injury are shared across solid organs, including the kidneys.[31] In the acute response initiated after insult to the kidney parenchyma and effector cells, injured tubular epithelia are activated. In the later phase, the ECM expansion occurs ultimately driving progression to fibrosis and organ dysfunction. The present study focused on the earlier phase and investigated the mechanisms underlying paracrine signaling from injured tubular epithelia to induce fibroblast mobilization toward the injury site in the acute phase after kidney injury *in vitro* and *in vivo*. We identified injured tubule-derived CCN1 as a strong candidate in a comparative transcriptomic analysis of injured tubular epithelia and CM from injured epithelia-treated fibroblasts. CCN1 is up-regulated earlier after injury, but its expression rapidly decreases thereafter, and its dynamics *in vivo* differed from those of well-known mediators involved in kidney fibrosis, such as TGF-β and CTGF. CCN1 regulates fibroblast chemotaxis and chemokinesis through FAK-ERK signaling *in vitro*. In addition, the loss of CCN1 expression in tubular epithelia diminished the mobilization of fibroblasts toward injured tissue *in vivo*, and the subsequent tissue fibrosis was inhibited in severe IRI. These findings suggest that CCN1 is specifically involved in the local accumulation of fibroblasts at injury sites in the earlier phase of the fibrogenic process, but it is indispensable for developing tissue fibrosis at later time points after severe AKI (Figure 7K).

CCN1 was initially identified as a cysteine-rich protein encoded by a growth factor-inducible immediate-early gene.[32] In the human adult kidney, CCN1 expression was observed in podocytes and whole segments of tubular epithelia including PTs.[33] In the IRI kidney, CCN1 has been shown to be rapidly up-regulated in the PTs at 1 h and its expression peaked between 12 and 24 h after injury.[22–24] Given this rapid increase in CCN1 expression after injury, urinary CCN1 is regarded as a candidate biomarker of injured PTs in the super acute phase of AKI.[34,35] Our results describing CCN1 expression dynamics after various kidney injuries also revealed its up-regulation in the earlier phase and a reduction in its expression thereafter, which is in contrast to other profibrotic factors. In addition, our results demonstrated that CCN1 did not up-regulate *Acta2* mRNA expression, a marker of myofibroblasts. These results suggest that the role of CCN1 is specific for the mobilization of fibroblasts toward injury sites in the acute phase after injury, and not necessarily for ECM production or the transdifferentiation of pericytes and fibroblasts to myofibroblasts.

Roles for CCN1 in tissue injury and repair processes have been examined in injury models of various organs yielding conflicting reports. Two studies from the same research group demonstrated that a neutralizing antibody against CCN1 ameliorated kidney fibrosis in the chronic phase of IRI and unilateral ureteral obstruction (UUO) kidneys.[24,25] In contrast, CCN1 has been reported to limit tissue fibrosis in other organs including in CCl4-induced or bile duct ligation-induced liver injury models,[36] in cutaneous wound healing models,[37] and in a dextran sodium sulfate-induced colitis model.[38] In liver fibrosis, CCN1 induced senescent phenotypes in surrounding fibroblasts, thereby reducing tissue fibrosis in the chronic phase after injury.[36] The results obtained herein from CCN1-KO mice suggested that the pro-fibrotic roles of CCN1 in the kidney depend on the severity of tissue injury. Given the small effect of CCN1 on the myofibroblast transdifferentiation and ECM synthesis in fibroblasts, CCN1 from injured tubules specifically acts as an alarm of the tissue injury, resulting in the fibroblast accumulation. In case of severe injury like 35 min IRI in our experiments, the profibrotic mediators like TGF-β or PDGF, which are subsequently released at the later time point, contribute to the maladaptive repair and tissue fibrosis.

Figure 4. The PT-specific knockout of CCN1 inhibits the accumulation of fibroblasts at injured tubules in cisplatin nephrotoxicity *in vivo*

(A) Experimental scheme. Tubular-specific CCN1 knockout mice (CCN1Flox/Flox SLC34a1GCE x R26tdTomato: CCN-KO) received intraperitoneal injections of cisplatin (15 mg/kg) and tamoxifen (3 mg/kg at each time point) as indicated.

(B) Histological analysis of the kidney after the cisplatin injection by immunostaining of KIM1.

(C) RT-PCR of the *Ccn1* and *Havcr1* genes in sorted tdTomato+ tubular epithelial cells.

(D) Changes in BUN after the administration of cisplatin. n = 7–8 per group.

(E) Representative co-immunofluorescence images of KIM1 and pFAK, PDGFRβ and pFAK, and PDGFRβ and γH2AX at 4 days after cisplatin injection.

(F) Representative images of Sirius red staining at 14 days after cisplatin injection.

(G) Semi-quantitative fibrosis scores. n = 9 WT Cis (−), n = 8 WT Cis (+), n = 7 CCN1-KO Cis (+).

(H) qPCR of RNA from whole kidneys as representative markers of myofibroblasts (*Acta2*), fibroblasts (*Pdgfrb*), profibrotic factor (*Tgfb1*), macrophage (*Cd68*), tubular injury (*Havcr1*), tubular integrity (*Lrp2*), and extracellular matrix (*Col1a1* and *Fn1*). n = 5 WT Cis (−), n = 8 WT Cis (+), n = 7 CCN1-KO Cis (+). The scale bars indicate 100 μm in (B), 50 μm in low-power field pictures, and 20 μm in high-power field pictures in (E). The scale bars indicate 50 μm in (F).

For all groups, data are means ± SEM. Statistical analyses were performed by unpaired t test for comparisons of two variables and by ANOVA and Dunnett's post hoc test for comparisons of multiple variables. $^{*}p < 0.05$.

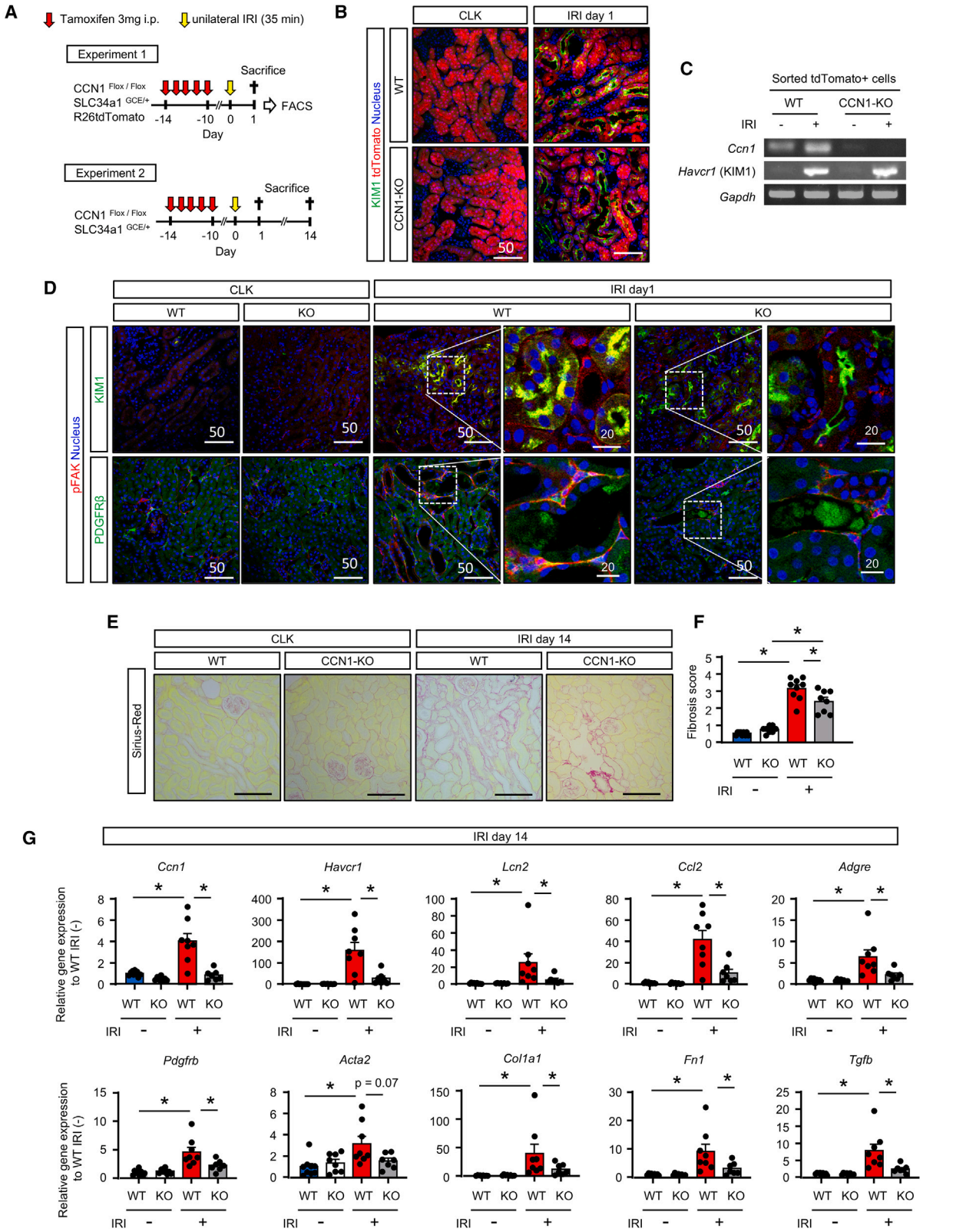

(legend on next page)

CCN1 has been shown to play a role in tissue injury and repair processes by interacting with disparate cell types through specific integrin receptors.[21,39] Based on a previous study showing that CCN1 activated FAK, leading to the migration of vascular smooth muscle cells,[40] and our transcriptomics data, we focused on FAK as a target signaling molecule of CCN1. FAK was initially described as a protein that is highly phosphorylated upon the clustering of integrins at focal adhesions.[41–43] We found that CCN1 phosphorylated FAK at the Tyr397 residue, which is the major FAK activation site.[44] FAK phosphorylation at Tyr397 allows its kinase domain to bind to various kinases, including Src,[45] phosphatidylinositol 3-kinase,[46] and phospholipase C-γ,[47] and these kinases may further activate downstream signaling, including ERK, eventually accelerating cell migration. We showed that the genetic ablation and pharmacological inhibition of FAK canceled fibroblast migration mediated by CCN1 and by CM from injured epithelia, suggesting that FAK phosphorylation at Tyr397 plays a central role in this process.

In conclusion, the present study revealed tubular epithelial cell-fibroblast interactions through the paracrine effects of CCN1 *in vitro* and *in vivo.* CCN1 up-regulation in tubular epithelia only occurred in the acute phase after injury, and injured tubule-derived CCN1 promoted the mobilization of fibroblasts into injury sites. In case of severe injury, subsequent up-regulation of other profibrotic mediators might contribute to the myofibroblast transdifferentiation and ECM synthesis. Therefore, inhibition of CCN1 can be an attractive therapeutic candidate to prevent the AKI to CKD transition; whether this strategy can be applied to other CKD models including UUO or repeated cisplatin injection model is unclear and, thus, further investigations are warranted.

Limitations of the study

There are several limitations in this study. We focused on the paracrine interaction between injured tubular epithelia and fibroblasts through CCN1; therefore, interactions with the other cell types have not been examined. In addition, recent research has demonstrated that fibroblasts also express CCN1.[48,49] Deletion of CCN1 in fibroblasts has been shown to reduce fibrous tissue in cancer and to cause qualitative changes in the ECM, including alterations in its amount and fibrous structure.[48] Following myocardial infarction, deletion of CCN1 in fibroblasts resulted in impaired fibrosis, which ultimately led to cardiac rupture.[49] While fibroblast-derived CCN1 has been shown to play critical roles in tissue remodeling and fibrosis in other organs, its function in renal tissue remains unclear. Although we demonstrated that c-fos/Jun/AP-1 signaling up-regulated CCN1 expression, the mechanisms by which CCN1 is down-regulated after tubular injury have yet to be elucidated. Based on the results of transcriptomics, we investigated the role of injured tubule-derived CCN1 in promoting fibroblast migration. However, it is well known that multiple humoral factors contribute to this process. Our transcriptomics also revealed the up-regulation of other humoral factors, such as CCN2, which are potentially involved in fibroblast migration, although we have not yet directly examined the individual and combined effects of these other factors on fibroblast migration. Since gender and genetic backgrounds including mouse strains affect the severity of kidney injury, whether our results can be generalized beyond these differences is unknown.

RESOURCE AVAILABILITY

Lead contact

Requests for further information and resources should be directed to and will be fulfilled by the lead contact, Dr. Tetsuro Kusaba (kusaba@koto.kpu-m.ac.jp).

Materials availability

This study did not generate new unique reagents.

Data and code availability

- All data reported in this paper will be shared by the lead contact upon request.
- This paper does not report the original code.
- RNA-seq data for all samples were deposited in the Gene Expression Omnibus under the accession number GSE248209.
- Any additional information required to reanalyze the data reported in this paper is available from the lead contact upon request.

ACKNOWLEDGMENTS

The authors would like to thank Prof. Lester F. Lau for his kind gift of CCN1-floxed mice.

AUTHOR CONTRIBUTIONS

T.N. and T. K. designed the study, performed the experiments, analyzed the data, and wrote the manuscript. Y.K. analyzed the data. M.U., M.A., and S. S. performed the experiments, and analyzed the data. A.M., H.Y-S., Y.S., Y.M., N.O-O, I.N., K.N., A.Y-T., N.Y., K.T, B.D.H., and S.M. contributed to the discussion.

Figure 5. The PT-specific knockout of CCN1 inhibits the accumulation of fibroblasts at injured tubules and subsequent tissue fibrosis in IRI *in vivo*

(A) Experimental scheme. Tubular-specific CCN1 knockout mice (CCN1Flox/Flox SLC34a1GCE x R26tdTomato: CCN-KO) received IRI (35 min) and tamoxifen (3 mg/kg at each time point) as indicated.

(B) Histological analysis of the kidney at 1 day after IRI by immunostaining of KIM1.

(C) RT-PCR of the *Ccn1* and *Havcr1* genes in sorted tdTomato+ tubular epithelial cells.

(D) Representative co-immunofluorescence images of KIM1 and pFAK, and PDGFRβ and pFAK at 1 day after IRI.

(E) Representative images of Sirius red staining.

(F) Semi-quantitative fibrosis scores at 14 days after IRI. n = 9 WT IRI (−), n = 8 WT IRI (+), n = 9 CCN1-KO IRI (−), n = 8 CCN1-KO IRI (+).

(G) qPCR of RNA from whole kidneys as representative markers of tubular injury (*Havcr1*), tubular integrity (*Lrp2*), chemokine (*Ccl2*), macrophage (*Cd68*), fibroblasts (*Pdgfrb*), myofibroblasts (*Acta2*), extracellular matrix (*Col1a1* and *Fn1*), and profibrotic factor (*Tgfb1*). n = 9 WT IRI (−), n = 8 WT IRI (+), n = 8 CCN1-KO IRI (−), n = 7 CCN1-KO IRI (+). The scale bars indicate 100 μm in (B), 50 μm in low-power field pictures, and 20 μm in high-power field pictures in (D). The scale bars indicate 50 μm in (E).

For all groups, data are means ± SEM. Statistical analyses were performed by paired t test for comparisons of IRI kidney and contralateral kidney (CLK) and by ANOVA and Dunnett's post hoc test for comparisons of multiple variables. $^*p < 0.05$.

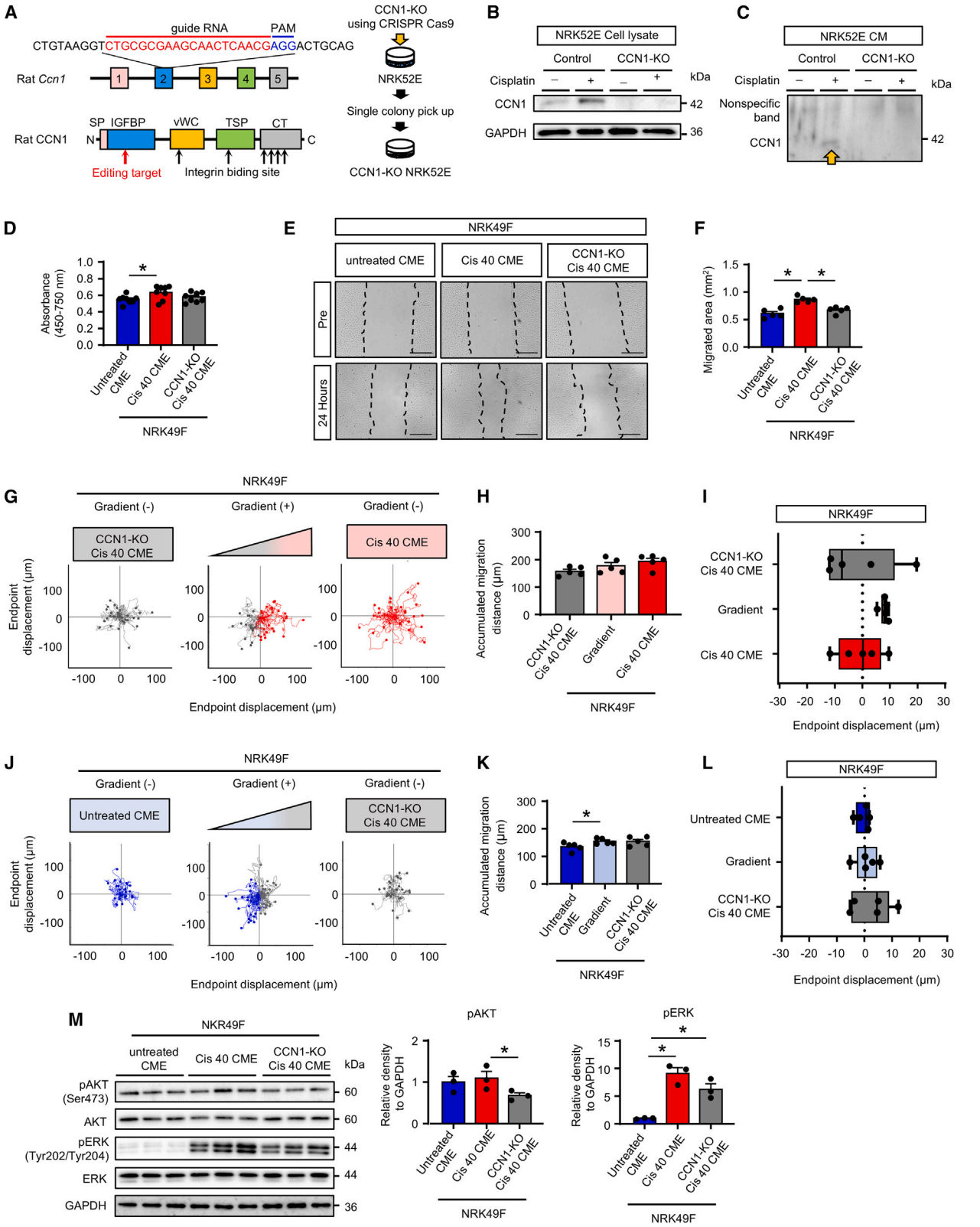

(legend on next page)

DECLARATION OF INTERESTS

The authors declare no competing interests.

STAR★METHODS

Detailed methods are provided in the online version of this paper and include the following:

- KEY RESOURCES TABLE
- EXPERIMENTAL MODEL AND STUDY PARTICIPANT DETAILS
  - Mice and ethics statement
  - SLC34a1GCE mice and CCN1 floxed mice
  - Cell culture
- METHOD DETAILS
  - Cisplatin-induced kidney injury model
  - Renal ischemia reperfusion injury model
  - Aristolochic acid nephropathy model
  - Unilateral ureteral obstruction model
  - Tissue preparation and histology
  - Separation of tdTomato-positive proximal tubular epithelia using FACS
  - Culture media (CM) collection
  - Cell proliferation assay
  - Scratch assay
  - Single cell migration assay
  - RNA extraction and real-time quantitative PCR
  - Western blot analysis
  - Knockdown by siRNA
  - KO of CCN1 in tubular epithelia by CRISPR-Cas9
  - Immunofluorescence analysis
  - Immunohistochemistry analysis
  - RNA sequencing (RNA-seq)
  - Bioinformatic analysis
  - Human *CCN1* expression analysis using published datasets
- QUANTIFICATION AND STATISTICAL ANALYSIS

SUPPLEMENTAL INFORMATION

Supplemental information can be found online at https://doi.org/10.1016/j.isci.2025.112176.

Received: December 1, 2024
Revised: January 28, 2025
Accepted: March 4, 2025
Published: March 7, 2025

REFERENCES

1. Venkatachalam, M.A., Weinberg, J.M., Kriz, W., and Bidani, A.K. (2015). Failed Tubule Recovery, AKI-CKD Transition, and Kidney Disease Progression. J. Am. Soc. Nephrol. *26*, 1765–1776. https://doi.org/10.1681/ASN.2015010006.
2. He, L., Wei, Q., Liu, J., Yi, M., Liu, Y., Liu, H., Sun, L., Peng, Y., Liu, F., Venkatachalam, M.A., and Dong, Z. (2017). AKI on CKD: heightened injury, suppressed repair, and the underlying mechanisms. Kidney Int. *92*, 1071–1083. https://doi.org/10.1016/j.kint.2017.06.030.
3. Goldstein, S.L., Jaber, B.L., Faubel, S., and Chawla, L.S.; Acute Kidney Injury Advisory Group of American Society of Nephrology (2013). AKI transition of care: a potential opportunity to detect and prevent CKD. Clin. J. Am. Soc. Nephrol. *8*, 476–483. https://doi.org/10.2215/CJN.12101112.
4. Qi, R., and Yang, C. (2018). Renal tubular epithelial cells: the neglected mediator of tubulointerstitial fibrosis after injury. Cell Death Dis. *9*, 1126. https://doi.org/10.1038/s41419-018-1157-x.
5. Yang, L., Besschetnova, T.Y., Brooks, C.R., Shah, J.V., and Bonventre, J.V. (2010). Epithelial cell cycle arrest in G2/M mediates kidney fibrosis after injury. Nat. Med. *16*, 535–543, 531p following 143. https://doi.org/10.1038/nm.2144.
6. Bonventre, J.V., and Yang, L. (2011). Cellular pathophysiology of ischemic acute kidney injury. J. Clin. Investig. *121*, 4210–4221. https://doi.org/10.1172/JCI45161.
7. Liu, B.C., Tang, T.T., Lv, L.L., and Lan, H.Y. (2018). Renal tubule injury: a driving force toward chronic kidney disease. Kidney Int. *93*, 568–579. https://doi.org/10.1016/j.kint.2017.09.033.
8. Venugopal, H., Hanna, A., Humeres, C., and Frangogiannis, N.G. (2022). Properties and Functions of Fibroblasts and Myofibroblasts in Myocardial Infarction. Cells *11*, 1386. https://doi.org/10.3390/cells11091386.
9. Kaissling, B., Lehir, M., and Kriz, W. (2013). Renal epithelial injury and fibrosis. Biochim. Biophys. Acta *1832*, 931–939. https://doi.org/10.1016/j.bbadis.2013.02.010.
10. Molkentin, J.D., Bugg, D., Ghearing, N., Dorn, L.E., Kim, P., Sargent, M.A., Gunaje, J., Otsu, K., and Davis, J. (2017). Fibroblast-Specific Genetic Manipulation of p38 Mitogen-Activated Protein Kinase In Vivo Reveals Its Central Regulatory Role in Fibrosis. Circulation *136*, 549–561. https://doi.org/10.1161/CIRCULATIONAHA.116.026238.
11. Shaw, T.J., and Martin, P. (2016). Wound repair: a showcase for cell plasticity and migration. Curr. Opin. Cell Biol. *42*, 29–37. https://doi.org/10.1016/j.ceb.2016.04.001.
12. Heymans, S., Luttun, A., Nuyens, D., Theilmeier, G., Creemers, E., Moons, L., Dyspersin, G.D., Cleutjens, J.P., Shipley, M., Angellilo, A., et al. (1999). Inhibition of plasminogen activators or matrix metalloproteinases prevents

Figure 6. Loss of CCN1 cancels the injured tubular epithelia-derived conditioned medium-mediated chemokinesis of fibroblasts

(A) Schematic illustration of the targeting strategy for the knockout of CCN1 in NRK52E by the CRISPR-Cas9 system.
(B) Western blot analysis of CCN1 in the cell lysate of CCN1-knocked out (KO) NRK52E.
(C) Western blot analysis of CCN1 in CME. The arrow indicates the target band.
(D) Cell proliferation assay data indicating that CCN1-KO CME NRK52E slightly suppressed the growth of NRK49F. $n = 8$ each.
(E) Representative pictures of the scratch migration assay of CCN1-KO CME-treated NRK49F. The scale bars indicate 500 μm.
(F) Quantification of the migrated area of NRK49F. $n = 5$ each.
(G) Representative pictures of polar plots displaying the trajectories of NRK49F migrating in CCN1-KO Cis 40-CME (left), in Cis 40-CME (right), and in gradients in between (middle). The gradient is formed from CCN1-KO Cis 40-CM on the left side to Cis 40-CME on the right side of the plots.
(H) Analysis of NRK49F migration by the average track diameter. $n = 5$ each compartment.
(I) Analysis of average endpoint displacements indicating that CCN1 is chemotactic. $n = 5$ each compartment.
(J) Representative pictures of polar plots displaying the trajectories of NRK49F migrating in untreated CME (left), in CCN1-KO Cis 40-CME (right), and in gradients in between (middle). The gradient is formed from untreated CME on the left side to CCN1-KO Cis 40-CME on the right side of the plots.
(K) Analysis of NRK49F migration by the average track diameter. $n = 5$ each compartment.
(L) Analysis of average endpoint displacements indicating CCN1 has chemotaxis. $n = 5$ each compartment.
(M) Western blot analysis of pAKT, AKT, pERK, ERK, and GAPDH in NRK49F treated with CCN1-KO Cis 40-CME for 30 min. The optical densities of the bands of pAKT and pERK were normalized against GAPDH. $n = 3$ each. All scratch migration assays or single-cell migration assays were performed after mitomycin pretreatment. For all groups, data are means ± SEM. Endpoint displacements in (I) and (L) are reported in a box and whisker plot. Statistical analyses were performed by unpaired t test for comparisons of two variables and by ANOVA and Dunnett's post hoc test for comparisons of multiple variables. $^*p < 0.05$.

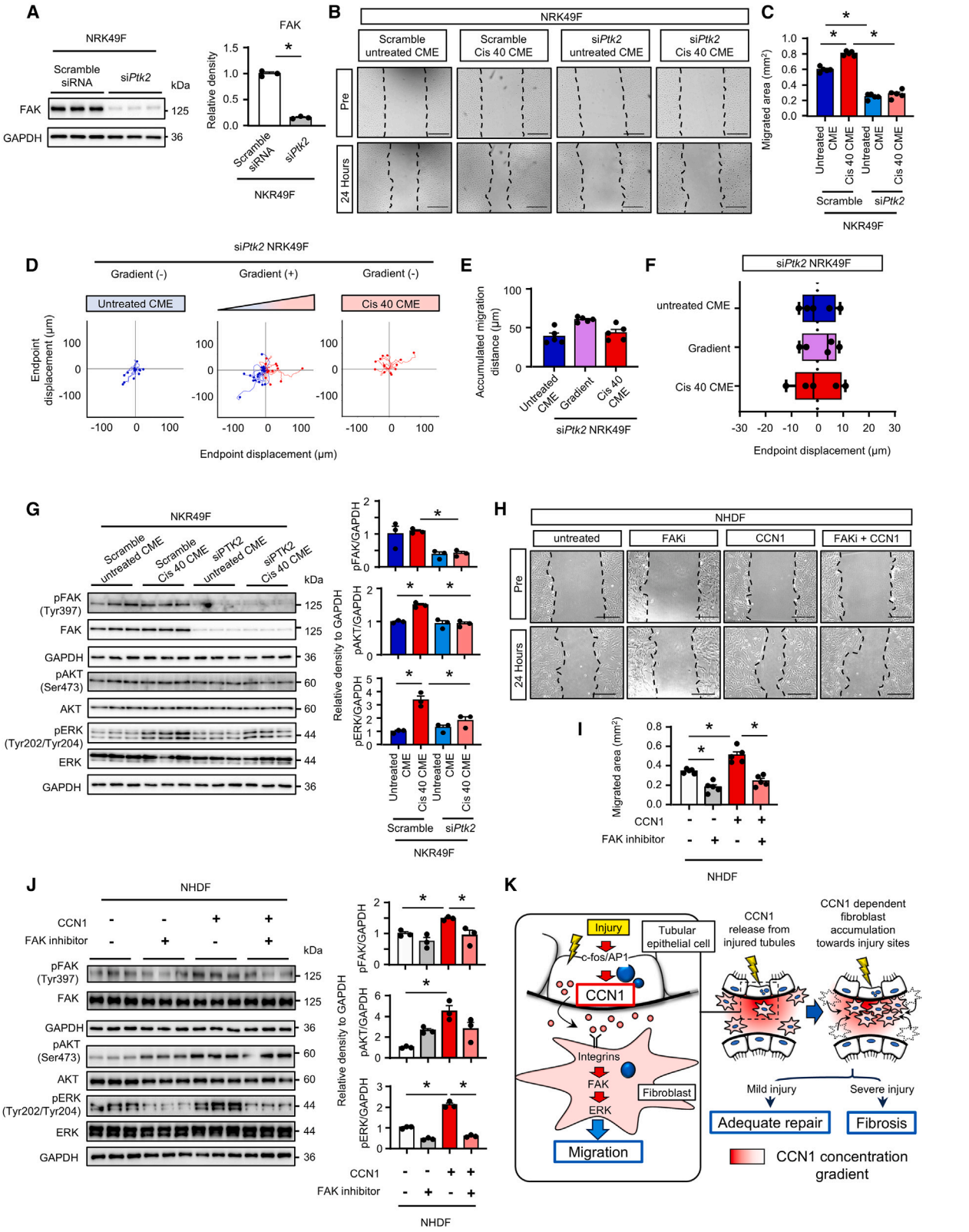

(legend on next page)

cardiac rupture but impairs therapeutic angiogenesis and causes cardiac failure. Nat. Med. *5*, 1135–1142. https://doi.org/10.1038/13459.

13. Kong, P., Shinde, A.V., Su, Y., Russo, I., Chen, B., Saxena, A., Conway, S.J., Graff, J.M., and Frangogiannis, N.G. (2018). Opposing Actions of Fibroblast and Cardiomyocyte Smad3 Signaling in the Infarcted Myocardium. Circulation *137*, 707–724. https://doi.org/10.1161/CIRCULATIONAHA.117.029622.
14. Burke, R.M., Burgos Villar, K.N., and Small, E.M. (2021). Fibroblast contributions to ischemic cardiac remodeling. Cell. Signal. *77*, 109824. https://doi.org/10.1016/j.cellsig.2020.109824.
15. Schiessl, I.M., Grill, A., Fremter, K., Steppan, D., Hellmuth, M.K., and Castrop, H. (2018). Renal Interstitial Platelet-Derived Growth Factor Receptor-beta Cells Support Proximal Tubular Regeneration. J. Am. Soc. Nephrol. *29*, 1383–1396. https://doi.org/10.1681/ASN.2017101069.
16. Nakamura, J., Sato, Y., Kitai, Y., Wajima, S., Yamamoto, S., Oguchi, A., Yamada, R., Kaneko, K., Kondo, M., Uchino, E., et al. (2019). Myofibroblasts acquire retinoic acid-producing ability during fibroblast-to-myofibroblast transition following kidney injury. Kidney Int. *95*, 526–539. https://doi.org/10.1016/j.kint.2018.10.017.
17. Buchtler, S., Grill, A., Hofmarksrichter, S., Stöckert, P., Schiechl-Brachner, G., Rodriguez Gomez, M., Neumayer, S., Schmidbauer, K., Talke, Y., Klinkhammer, B.M., et al. (2018). Cellular Origin and Functional Relevance of Collagen I Production in the Kidney. J. Am. Soc. Nephrol. *29*, 1859–1873. https://doi.org/10.1681/ASN.2018020138.
18. Kishi, S., Brooks, C.R., Taguchi, K., Ichimura, T., Mori, Y., Akinfolarin, A., Gupta, N., Galichon, P., Elias, B.C., Suzuki, T., et al. (2019). Proximal tubule ATR regulates DNA repair to prevent maladaptive renal injury responses. J. Clin. Investig. *129*, 4797–4816. https://doi.org/10.1172/JCI122313.
19. Gewin, L., Zent, R., and Pozzi, A. (2017). Progression of chronic kidney disease: too much cellular talk causes damage. Kidney Int. *91*, 552–560. https://doi.org/10.1016/j.kint.2016.08.025.
20. Tan, R.J., Zhou, D., and Liu, Y. (2016). Signaling Crosstalk between Tubular Epithelial Cells and Interstitial Fibroblasts after Kidney Injury. Kidney Dis. *2*, 136–144. https://doi.org/10.1159/000446336.
21. Kim, K.H., Won, J.H., Cheng, N., and Lau, L.F. (2018). The matricellular protein CCN1 in tissue injury repair. J. Cell Commun. Signal. *12*, 273–279. https://doi.org/10.1007/s12079-018-0450-x.
22. Kirita, Y., Wu, H., Uchimura, K., Wilson, P.C., and Humphreys, B.D. (2020). Cell profiling of mouse acute kidney injury reveals conserved cellular responses to injury. Proc. Natl. Acad. Sci. USA *117*, 15874–15883. https://doi.org/10.1073/pnas.2005477117.
23. Muramatsu, Y., Tsujie, M., Kohda, Y., Pham, B., Perantoni, A.O., Zhao, H., Jo, S.K., Yuen, P.S.T., Craig, L., Hu, X., and Star, R.A. (2002). Early detection of cysteine rich protein 61 (CYR61, CCN1) in urine following renal ischemic reperfusion injury. Kidney Int. *62*, 1601–1610. https://doi.org/10.1046/j.1523-1755.2002.00633.x.
24. Lai, C.F., Lin, S.L., Chiang, W.C., Chen, Y.M., Wu, V.C., Young, G.H., Ko, W.J., Kuo, M.L., Tsai, T.J., and Wu, K.D. (2014). Blockade of cysteine-rich protein 61 attenuates renal inflammation and fibrosis after ischemic kidney injury. Am. J. Physiol. Renal Physiol. *307*, F581–F592. https://doi.org/10.1152/ajprenal.00670.2013.
25. Lai, C.F., Chen, Y.M., Chiang, W.C., Lin, S.L., Kuo, M.L., and Tsai, T.J. (2013). Cysteine-rich protein 61 plays a proinflammatory role in obstructive kidney fibrosis. PLoS One *8*, e56481. https://doi.org/10.1371/journal.pone.0056481.
26. Kingham, P.J., and Pocock, J.M. (2001). Microglial secreted cathepsin B induces neuronal apoptosis. J. Neurochem. *76*, 1475–1484. https://doi.org/10.1046/j.1471-4159.2001.00146.x.
27. Kusaba, T., Lalli, M., Kramann, R., Kobayashi, A., and Humphreys, B.D. (2014). Differentiated kidney epithelial cells repair injured proximal tubule. Proc. Natl. Acad. Sci. USA *111*, 1527–1532. https://doi.org/10.1073/pnas.1310653110.
28. Cippa, P.E., Sun, B., Liu, J., Chen, L., Naesens, M., and McMahon, A.P. (2018). Transcriptional trajectories of human kidney injury progression. JCI Insight *3*, e123151. https://doi.org/10.1172/jci.insight.123151.
29. Lake, B.B., Menon, R., Winfree, S., Hu, Q., Melo Ferreira, R., Kalhor, K., Barwinska, D., Otto, E.A., Ferkowicz, M., Diep, D., et al. (2023). An atlas of healthy and injured cell states and niches in the human kidney. Nature *619*, 585–594. https://doi.org/10.1038/s41586-023-05769-3.
30. Huang, T.L., Mu, N., Gu, J.T., Shu, Z., Zhang, K., Zhao, J.K., Zhang, C., Hao, Q., Li, W.N., Zhang, W.Q., et al. (2017). DDR2-CYR61-MMP1 Signaling Pathway Promotes Bone Erosion in Rheumatoid Arthritis Through Regulating Migration and Invasion of Fibroblast-Like Synoviocytes. J. Bone Miner. Res. *32*, 407–418. https://doi.org/10.1002/jbmr.2993.
31. Rockey, D.C., Bell, P.D., and Hill, J.A. (2015). Fibrosis–a common pathway to organ injury and failure. N. Engl. J. Med. *372*, 1138–1149. https://doi.org/10.1056/NEJMra1300575.
32. O'Brien, T.P., Yang, G.P., Sanders, L., and Lau, L.F. (1990). Expression of cyr61, a growth factor-inducible immediate-early gene. Mol. Cell Biol. *10*, 3569–3577. https://doi.org/10.1128/mcb.10.7.3569-3577.1990.
33. Sawai, K., Mukoyama, M., Mori, K., Kasahara, M., Koshikawa, M., Yokoi, H., Yoshioka, T., Ogawa, Y., Sugawara, A., Nishiyama, H., et al. (2007). Expression of CCN1 (CYR61) in developing, normal, and diseased human

Figure 7. FAK inhibition cancels the CCN1-mediated chemokinesis of fibroblasts

(A) Western blot analysis of FAK in NRK49F knocked down by Duplexed Silencer Select RNA inhibition against protein tyrosine kinase 2 (*Ptk2*). The optical densities of FAK bands were normalized against GAPDH. $n = 3$ each.

(B) Representative pictures of the scratch migration assay of NRK49F with the knockdown of *Ptk2*. The scale bars indicate 500 μm.

(C) Quantification of the migrated area of NRK49F. $n = 5$ each.

(D) Representative pictures of polar plots displaying the trajectories of si*Ptk2* NRK49F migrating in untreated CME (left), in Cis 40-CME (right), and in gradients in between (middle). The gradient is formed from untreated CME on the left side to Cis 40-CME on the right side of the plots.

(E) Analysis of si*Ptk2* NRK49F migration by the average track diameter. $n = 5$ each compartment.

(F) Analysis of average endpoint displacements indicating chemotaxis loss by the knockdown of *Ptk2* expression. $n = 5$ each compartment.

(G) Western blot analysis of pFAK, FAK, and GAPDH in si*Ptk2* NRK49F treated with Cis 40-CME for 10 min. Western blot analysis of pAKT, AKT, pERK, ERK, and GAPDH in si*Ptk2* NRK49F treated with Cis 40-CME for 30 min. The optical densities of the bands of these molecules were normalized against GAPDH. $n = 3$ each.

(H) Representative pictures of the scratch migration assay of NHDF treated with the FAK inhibitor and CCN1. The scale bars indicate 500 μm.

(I) Quantification of the migrated area of NHDF. $n = 5$ each.

(J) Western blot analysis of pFAK, FAK, and GAPDH in NHDF treated with the FAK inhibitor and CCN1 10 min after treatments. Western blot analysis of pAKT, AKT, pERK, ERK, and GAPDH in NHDF treated with the FAK inhibitor and CCN1 for 30 min. The optical densities of the bands of these molecules were normalized against GAPDH. $n = 3$ each.

(K) Scheme of the proposed role of injured tubule-derived CCN1 on interstitial fibroblasts in AKI. All scratch migration assays or single-cell migration assays were performed after mitomycin pretreatment.

For all groups, data are means ± SEM. Endpoint displacements in (F) are reported in a box and whisker plot. Statistical analyses were performed by unpaired t test for comparisons of two variables and by ANOVA and Dunnett's post hoc test for comparisons of multiple variables. $^*p < 0.05$.

kidney. Am. J. Physiol. Renal Physiol. *293*, F1363–F1372. https://doi.org/10.1152/ajprenal.00205.2007.

34. Li, C., Zhao, L., Wang, Y., Che, L., Luan, H., Luo, C., and Xu, Y. (2019). Cysteine-rich protein 61, a specific ultra-early biomarker in kidney ischemia/reperfusion injury. Nephrology *24*, 798–805. https://doi.org/10.1111/nep.13513.
35. Bonventre, J.V., Vaidya, V.S., Schmouder, R., Feig, P., and Dieterle, F. (2010). Next-generation biomarkers for detecting kidney toxicity. Nat. Biotechnol. *28*, 436–440. https://doi.org/10.1038/nbt0510-436.
36. Kim, K.H., Chen, C.C., Monzon, R.I., and Lau, L.F. (2013). Matricellular protein CCN1 promotes regression of liver fibrosis through induction of cellular senescence in hepatic myofibroblasts. Mol. Cell Biol. *33*, 2078–2090. https://doi.org/10.1128/MCB.00049-13.
37. Jun, J.I., and Lau, L.F. (2010). The matricellular protein CCN1 induces fibroblast senescence and restricts fibrosis in cutaneous wound healing. Nat. Cell Biol. *12*, 676–685. https://doi.org/10.1038/ncb2070.
38. Choi, J.S., Kim, K.H., and Lau, L.F. (2015). The matricellular protein CCN1 promotes mucosal healing in murine colitis through IL-6. Mucosal Immunol. *8*, 1285–1296. https://doi.org/10.1038/mi.2015.19.
39. Lau, L.F. (2016). Cell surface receptors for CCN proteins. J. Cell Commun. Signal. *10*, 121–127. https://doi.org/10.1007/s12079-016-0324-z.
40. Wu, D.D., Zhang, F., Hao, F., Chun, J., Xu, X., and Cui, M.Z. (2014). Matricellular protein Cyr61 bridges lysophosphatidic acid and integrin pathways leading to cell migration. J. Biol. Chem. *289*, 5774–5783. https://doi.org/10.1074/jbc.M113.533042.
41. Kanner, S.B., Reynolds, A.B., Vines, R.R., and Parsons, J.T. (1990). Monoclonal antibodies to individual tyrosine-phosphorylated protein substrates of oncogene-encoded tyrosine kinases. Proc. Natl. Acad. Sci. USA *87*, 3328–3332. https://doi.org/10.1073/pnas.87.9.3328.
42. Lipfert, L., Haimovich, B., Schaller, M.D., Cobb, B.S., Parsons, J.T., and Brugge, J.S. (1992). Integrin-dependent phosphorylation and activation of the protein tyrosine kinase pp125FAK in platelets. J. Cell Biol. *119*, 905–912. https://doi.org/10.1083/jcb.119.4.905.
43. Schaller, M.D., Borgman, C.A., Cobb, B.S., Vines, R.R., Reynolds, A.B., and Parsons, J.T. (1992). pp125FAK a structurally distinctive protein-tyrosine kinase associated with focal adhesions. Proc. Natl. Acad. Sci. USA *89*, 5192–5196. https://doi.org/10.1073/pnas.89.11.5192.
44. Mousson, A., Sick, E., Carl, P., Dujardin, D., De Mey, J., and Rondé, P. (2018). Targeting Focal Adhesion Kinase Using Inhibitors of Protein-Protein Interactions. Cancers *10*, 278. https://doi.org/10.3390/cancers10090278.
45. Xing, Z., Chen, H.C., Nowlen, J.K., Taylor, S.J., Shalloway, D., and Guan, J.L. (1994). Direct interaction of v-Src with the focal adhesion kinase mediated by the Src SH2 domain. Mol. Biol. Cell *5*, 413–421. https://doi.org/10.1091/mbc.5.4.413.
46. Chen, H.C., and Guan, J.L. (1994). Association of focal adhesion kinase with its potential substrate phosphatidylinositol 3-kinase. Proc. Natl. Acad. Sci. USA *91*, 10148–10152. https://doi.org/10.1073/pnas.91.21.10148.
47. Zhang, X., Chattopadhyay, A., Ji, Q.S., Owen, J.D., Ruest, P.J., Carpenter, G., and Hanks, S.K. (1999). Focal adhesion kinase promotes phospholipase C-gamma1 activity. Proc. Natl. Acad. Sci. USA *96*, 9021–9026. https://doi.org/10.1073/pnas.96.16.9021.
48. Hutchenreuther, J., Nguyen, J., Quesnel, K., Vincent, K.M., Petitjean, L., Bourgeois, S., Boyd, M., Bou-Gharios, G., Postovit, L.M., and Leask, A. (2024). Cancer-associated Fibroblast-specific Expression of the Matricellular Protein CCN1 Coordinates Neovascularization and Stroma Deposition in Melanoma Metastasis. Cancer Res. Commun. *4*, 556–570. https://doi.org/10.1158/2767-9764.CRC-23-0571.
49. Fischer, A.G., Elliott, E.M., Brittian, K.R., Garrett, L., Sadri, G., Aebersold, J., Singhal, R.A., Nong, Y., Leask, A., Jones, S.P., and Moore Iv, J.B. (2024). Matricellular protein CCN1 promotes collagen alignment and scar integrity after myocardial infarction. Matrix Biol. *133*, 14–32. https://doi.org/10.1016/j.matbio.2024.08.001.
50. Uehara, M., Kusaba, T., Ida, T., Nakai, K., Nakata, T., Tomita, A., Watanabe-Uehara, N., Ikeda, K., Kitani, T., Yamashita, N., et al. (2020). Pharmacological inhibition of ataxia-telangiectasia mutated exacerbates acute kidney injury by activating p53 signaling in mice. Sci. Rep. *10*, 4441. https://doi.org/10.1038/s41598-020-61456-7.
51. Yamashita, N., Nakai, K., Nakata, T., Nakamura, I., Kirita, Y., Matoba, S., Humphreys, B.D., Tamagaki, K., and Kusaba, T. (2021). Cumulative DNA damage by repeated low-dose cisplatin injection promotes the transition of acute to chronic kidney injury in mice. Sci. Rep. *11*, 20920. https://doi.org/10.1038/s41598-021-00392-6.
52. Yamashita, N., Kusaba, T., Nakata, T., Tomita, A., Ida, T., Watanabe-Uehara, N., Ikeda, K., Kitani, T., Uehara, M., Kirita, Y., et al. (2020). Intratubular epithelial-mesenchymal transition and tubular atrophy after kidney injury in mice. Am. J. Physiol. Renal Physiol. *319*, F579–F591. https://doi.org/10.1152/ajprenal.00108.2020.
53. Zhou, Q., Jiang, L., Su, T., Liu, G., and Yang, L. (2023). Overview of aristolochic acid nephropathy: an update. Kidney Res. Clin. Pract. *42*, 579–590. https://doi.org/10.23876/j.krcp.22.211.
54. Kramann, R., Machado, F., Wu, H., Kusaba, T., Hoeft, K., Schneider, R.K., and Humphreys, B.D. (2018). Parabiosis and single-cell RNA sequencing reveal a limited contribution of monocytes to myofibroblasts in kidney fibrosis. JCI Insight *3*, e99561. https://doi.org/10.1172/jci.insight.99561.
55. Maarouf, O.H., Aravamudhan, A., Rangarajan, D., Kusaba, T., Zhang, V., Welborn, J., Gauvin, D., Hou, X., Kramann, R., and Humphreys, B.D. (2016). Paracrine Wnt1 Drives Interstitial Fibrosis without Inflammation by Tubulointerstitial Cross-Talk. J. Am. Soc. Nephrol. *27*, 781–790. https://doi.org/10.1681/ASN.2014121188.
56. Tomita-Yagi, A., Ozeki-Okuno, N., Watanabe-Uehara, N., Komaki, K., Umehara, M., Sawada-Yamauchi, H., Minamida, A., Sunahara, Y., Matoba, Y., Nakamura, I., et al. (2024). The importance of proinflammatory failed-repair tubular epithelia as a predictor of diabetic kidney disease progression. iScience *27*, 109020. https://doi.org/10.1016/j.isci.2024.109020.
57. Kitani, T., Kidokoro, K., Nakata, T., Kirita, Y., Nakamura, I., Nakai, K., Yagi-Tomita, A., Ida, T., Uehara-Watanabe, N., Ikeda, K., et al. (2022). Kidney vascular congestion exacerbates acute kidney injury in mice. Kidney Int. *101*, 551–562. https://doi.org/10.1016/j.kint.2021.11.015.
58. Uehara-Watanabe, N., Okuno-Ozeki, N., Minamida, A., Nakamura, I., Nakata, T., Nakai, K., Yagi-Tomita, A., Ida, T., Ikeda, K., Kitani, T., et al. (2022). Direct evidence of proximal tubular proliferation in early diabetic nephropathy. Sci. Rep. *12*, 778. https://doi.org/10.1038/s41598-022-04880-1.
59. Uehara-Watanabe, N., Okuno-Ozeki, N., Nakamura, I., Nakata, T., Nakai, K., Yagi-Tomita, A., Ida, T., Yamashita, N., Kamezaki, M., Kirita, Y., et al. (2022). Proximal tubular epithelia-specific transcriptomics of diabetic mice treated with dapagliflozin. Heliyon *8*, e10615. https://doi.org/10.1016/j.heliyon.2022.e10615.
60. Massena, S., Christoffersson, G., Vågesjö, E., Seignez, C., Gustafsson, K., Binet, F., Herrera Hidalgo, C., Giraud, A., Lomei, J., Weström, S., et al. (2015). Identification and characterization of VEGF-A-responsive neutrophils expressing CD49d, VEGFR1, and CXCR4 in mice and humans. Blood *126*, 2016–2026. https://doi.org/10.1182/blood-2015-03-631572.
61. Nakanishi, N., Ogata, T., Naito, D., Miyagawa, K., Taniguchi, T., Hamaoka, T., Maruyama, N., Kasahara, T., Nishi, M., Matoba, S., and Ueyama, T. (2016). MURC deficiency in smooth muscle attenuates pulmonary hypertension. Nat. Commun. *7*, 12417. https://doi.org/10.1038/ncomms12417.
62. Rothblum, L.I., Rothblum, K., and Chang, E. (2017). PAF53 is essential in mammalian cells: CRISPR/Cas9 fails to eliminate PAF53 expression. Gene *612*, 55–60. https://doi.org/10.1016/j.gene.2016.12.023.

63. Labun, K., Montague, T.G., Gagnon, J.A., Thyme, S.B., and Valen, E. (2016). CHOPCHOP v2: a web tool for the next generation of CRISPR genome engineering. Nucleic Acids Res. *44*, W272–W276. https://doi.org/10.1093/nar/gkw398.

64. Ikeda, K., Kusaba, T., Tomita, A., Watanabe-Uehara, N., Ida, T., Kitani, T., Yamashita, N., Uehara, M., Matoba, S., Yamada, T., and Tamagaki, K. (2020). Diverse Receptor Tyrosine Kinase Phosphorylation in Urine-Derived Tubular Epithelial Cells from Autosomal Dominant Polycystic Kidney Disease Patients. Nephron *144*, 525–536. https://doi.org/10.1159/000509419.

65. Robinson, M.D., McCarthy, D.J., and Smyth, G.K. (2010). edgeR: a Bioconductor package for differential expression analysis of digital gene expression data. Bioinformatics *26*, 139–140. https://doi.org/10.1093/bioinformatics/btp616.

STAR★METHODS

KEY RESOURCES TABLE

REAGENT or RESOURCE	SOURCE	IDENTIFIER
Antibodies		
Phospho-Histone H2AX (Ser139)	Cell Signaling Technology	Cat# 2577S; RRID:AB_2118010
Cleaved Caspase-3	Cell Signaling Technology	Cat# 9664; RRID:AB_2070042
Phospho-AKT (Ser473)	Cell Signaling Technology	Cat# 9271; RRID:AB_329825
AKT	Cell Signaling Technology	Cat# 9272; RRID:AB_329827
Phospho-ERK (Thr202/Tyr204)	Cell Signaling Technology	Cat# 9101; RRID:AB_331646
ERK	Cell Signaling Technology	Cat# 9102; RRID:AB_330744
CCN1	abcam	Cat# ab24448
Phospho-FAK (phospho Y397)	abcam	Cat# ab82298
FAK	abcam	Cat# ab40794
GAPDH (HRP-conjugate)	abcam	Cat# ab105428
anti-rabbit antibody (HRP-Conjugated)	abcam	Cat# ab236469
KIM-1	R&D systems	Cat# AF1817; RRID:AB_2116446
FITC-conjugated anti-Lotus tetragonolobus lectin (LTL) antibody	Vector Labs	Cat# FL1321
Phalloidin rhodamine	Sigma-Aldrich	Cat# P1951
Anti-PDGFRβ antibody	eBioscience	Cat# 63-1402-82
Goat anti-Rabbit IgG (H+L) Cross-Adsorbed Secondary Antibody, Alexa Fluor™ 488	Invitrogen	Cat# A-11008
Goat anti-Rat IgG (H+L) Cross-Adsorbed Secondary Antibody, Alexa Fluor™ 488	Invitrogen	Cat# A-11006
Goat anti-Rabbit IgG (H+L) Cross-Adsorbed Secondary Antibody, Alexa Fluor™ 594	Invitrogen	Cat# A-11012
Bacterial and virus strains		
lenti CRISPR V2	addgene	#52961
Chemicals, peptides, and recombinant proteins		
Cisplatin	Nippon Kayaku	Code# 4291401A2093
Tamoxifen	Sigma-Aldrich	Cat# T5648
Aristolochic acid	Sigma-Aldrich	Cat# A5512
Human recombinant CCN1	Peprotech	Cat# # 120-25
Mitomycin C	FUJIFILM Wako	139-18711
GSK2256098 (FAK inhibitor)	Selleck Biotech	S8523
SCH772984 (ERK inhibitor)	Selleck Biotech	S7101
T-5224 (cFos/AP1 inhibitor)	Selleck Biotech	S8966
Silencer Select RNA inhibition against protein tyrosine kinase 2 (*Ptk2*)	Invitrogen	Cat# 4390771
Silencer Select Negative Control	Invitrogen	Cat# 4390843
Lipofectamine RNAiMAX reagent	Invitrogen	Cat# 13778150
Puromycin	Gibco	Cat #A1113802
4% Paraformaldehyde Phosphate Buffer Saluting	FUJIFILM Wako	Code# 163-20145
Phosphate Buffered Saline	Takara Bio	Cat# T9181
Sucrose	FUJIFILM Wako	Code# 196-00015
Optimum cutting temperature compound	Sakura Finetek Japan Co., Ltd	Code# 4583
Albumin.Bovine serum (BSA)	NAKALAI TESQUE	Code# 01860-07

(*Continued on next page*)

Continued

REAGENT or RESOURCE	SOURCE	IDENTIFIER
Fetal Bovine Serum (FBS)	Gibco	10270106
DAPI Fluoromount-G	Southern Biotech	Cat# 0100-20
Dulbecco's Minimal Essential Medium	FUJIFILM Wako	Code# 04330085
Lysing Buffer 17	R&D systems	Cat# 895943
Immobilon-P	Millipore	Cat# IPVH00010
ECL select Western blot detection reagent	GE Healthcare UK Ltd	Cat# RPN2235
Clarity MAX Western ECL substrate	Bio-Rad Laboratories, Inc.	Cat# 1705062
TRIzol	Life Technologies	N/A
Liberase TL	Sigma-Aldrich	5401020001
DNAse Inhibitor	Sigma-Aldrich	D5025
Diaminobenzidine chromogenic substrate	Agilent Technologies	K3468
DRAQ5	BioStatus	DR50050
Gelatin solution	Sigma-Aldrich	G1393
Critical commercial assays		
Direct-zol RNA miniprep	Zymo Research Corporation	Cat# R2051
PrimeScript RT reagent Kit	Takara Bio Inc.	N/A
KAPA SYBR FAST qPCR Master Mix	Kapa Biosystems	KK4602
EXPOSE Rabbit Specific HRP/DAB Detection IHC Kit	Abcam	Cat# 80437
Premix WST-1 Cell Proliferation Assay System	Takara Bio Inc.	Code# MK400
TruSeq-stranded mRNA sample prep kit	Illumina	Cat# 2020595
MycoAlert	Lonza	LT07-118
CellDirector 2D	Gradientech	11-001-10
Deposited data		
RNA-seq	This paper	https://www.ncbi.nlm.nih.gov/geo/ accession number: GSE248209
Experimental models: Cell lines		
Rat kidney fibroblast cells (NRF49F cells)	The JCRB Cell Bank	N/A
Rat kidney epithelial cells (NRK52E cells)	The JCRB Cell Bank	N/A
Normal Human Dermal Fibroblasts (NHDF)	Lonza	CC-2511
Lenti-X 293Tcells	Clontech	N/A
Experimental models: Organisms/strains		
Mouse: C57BL/6 mice	Shimizu, Inc.	N/A
Mouse: SLC34a1GCE mice	Harvard Univ	N/A
Mouse: C57BL/6 strain R26tdTomato reporter mice	Harvard Univ	N/A
Mouse: CCN1 floxed mice	Illinois Univ.	N/A
Oligonucleotides		
Primers see Table S3		
Recombinant DNA		
plenti CRISPR v2	Addgene	#52961
Software and algorithms		
Image J	National Institutes of Health	Java.version: 1.8.0_391
BZ-X800	Keyence	BZ Series Application 01.02.03.02
Thermal Cycler Dice Real Time System	Takara Bio Inc.	N/A
Bio-Rad CFX Maestro	Bio-Rad Laboratories, Inc	Version:4.1.2433. 1219

(*Continued on next page*)

Continued

REAGENT or RESOURCE	SOURCE	IDENTIFIER
PRISM	GraphPad Software	Version 8.4.3
FV1000(confocal microscopy)	Olympus	N/A
Eclipse E600 microscope	Nikon Corporation	N/A
SH800	SONY	N/A
R software	Free Software Foundation's GNU General Public License	https://www.R-project.org/
STAR (alexdobin/STAR: RNA-seq aligner)	GitHub	https://github.com/alexdobin/STAR/
Subread package	Subread	https://subread.sourceforge.net
Seurat	Satija Lab	Version:4.3.0
Tracking Tool PRO (Tracking Tool software)	Gradientech	https://gradientech.se
Juli Stage	Nano Entech	N/A

EXPERIMENTAL MODEL AND STUDY PARTICIPANT DETAILS

Mice and ethics statement

Experiments were conducted using 8-10 weeks male mice based on their availability. Littermate mice were randomly allocated to each experimental group. Mice were housed under pathogen-free conditions (temperature, 25°C; 12-h light/dark cycle) and had free access to normal chow and water. Each experimental group contained 5 mice. All experiments were approved by the Experimental Animals Committee, Kyoto Prefectural University of Medicine (Approval #2024-151), and were performed in accordance with the institutional guidelines and Guidelines for Proper Conduct of Animal Experiments by the Science Council of Japan.

SLC34a1GCE mice and CCN1 floxed mice

We recently generated mice with the CreERT2 cassette in the SLC34a1 locus, which enables the expression of Cre recombinase in proximal tubules after the injection of tamoxifen.[27] SLC34a1GCE mice were crossed with R26tdTomato reporter mice, in which tdTomato is expressed after the Cre-mediated recombination of the floxed stop cassette to obtain bigenic offspring. Regarding genetic labeling, tamoxifen (Sigma-Aldrich, St. Louis, MO) was dissolved in 3% (vol/vol) ethanol containing corn oil (Sigma-Aldrich) at a concentration of 10 mg/mL. Tamoxifen was intraperitoneally injected at the indicated dose on 5 consecutive days. We generated tubular-specific Ccn1 knockout mice (CCN1-KO) by crossing SLC34a1GCE mice and homozygous CCN1 floxed mice (a gift from Prof. Lester F Lau in Illinois Univ., USA).[36,37]

Cell culture

Normal rat kidney epithelial cells (NRK52E) and normal rat kidney fibroblasts (NRK49F) were obtained from the JCRB Cell Bank. NRK52E and NRK49F were cultured in DMEM (Wako, Osaka, Japan) containing 1% penicillin and streptomycin (Invitrogen, Carlsbad, CA) and 5% FBS (Gibco) at 37°C in a humidified 5% CO_2 and 95% air atmosphere. Normal human dermal fibroblasts (NHDF) were purchased from Lonza (Walkersville, MD, USA). NHDF and Lenti-X 293T cells (Clontech) were cultured in DMEM (Fujifilm Wako, Osaka, Japan) containing 1% penicillin and streptomycin (Invitrogen, Carlsbad, CA) and 10% FBS (Gibco) at 37°C in a humidified 5% CO_2 and 95% air atmosphere. At the indicated time points, human recombinant CCN1 (PeproTech, Rocky Hill, NJ, USA), the focal adhesion kinase (FAK) inhibitor GSK2256098 (Selleck Biotech, Houston, TX), the ERK inhibitor SCH772984 (Selleck Biotech, Houston, TX), or vehicle was added to the medium. All cells used in this study were tested regularly for mycoplasma contamination by MycoAlert (Lonza, Walkersville, MD, USA).

METHOD DETAILS

Cisplatin-induced kidney injury model

The cisplatin injury model was induced by an intraperitoneal injection of cisplatin (Nippon Kayaku, Tokyo, Japan) at a concentration of 15 mg/kg body weight into mice at the age of 9-10 weeks as previously described.[50,51] Mice were euthanized at the indicated time points after the cisplatin injection.

Renal ischemia reperfusion injury model

To generate an ischemia reperfusion injury (IRI) model, at the age of 9-10 weeks, male mice were anesthetized with pentobarbital and unilateral IRI was performed. Ischemia was induced by the retroperitoneal approach on the left kidney for 26 min (mild IRI) or 35 min (severe IRI) at 37°C as previously described.[27,52] Regarding volume supplementation, 0.5 ml of saline was injected intraperitoneally after surgery. At indicated timepoints after IRI surgery, mice were anesthetized with isoflurane and euthanized.

CellPress
OPEN ACCESS

Aristolochic acid nephropathy model

To generate an aristolochic acid nephropathy model, 8-week-old male mice were intraperitoneally injected with 5 mg/kg of aristolochic acid (Sigma-Aldrich) in DMSO vehicle on two consecutive days as previously described.[53] Control mice were treated with the same dosage of DMSO vehicle via intraperitoneal injections. Mice were euthanized 14 days after aristolochic acid injections.

Unilateral ureteral obstruction model

To generate a unilateral ureteral obstruction (UUO) model, at the age of 8-10 weeks, male mice were anesthetized with pentobarbital and the left ureter was ligated with 5-0 silk at 2 points. The kidneys were excised 3, 7, and 14 days after surgery as previously described.[54,55]

Tissue preparation and histology

Mice were anesthetized and sacrificed, and the kidneys were removed at the indicated time points. To obtain frozen sections, kidneys were fixed with 4% paraformaldehyde (Wako Pure Chemical Industries, Ltd., Osaka, Japan) for 1 hour on ice, incubated in 30% (vol/vol) sucrose in PBS at 4°C overnight, embedded in optimum cutting temperature compound (Sakura Finetek Japan Co., Ltd., Tokyo, Japan), and cut into 7-μm-thick sections. To obtain paraffin sections, kidneys were fixed with 4% paraformaldehyde and embedded in paraffin by Applied Medical Research Laboratory (Osaka, Japan). Paraffin-embedded mouse tissues were cut into 4-μm-thick sections. Periodic acid-Schiff, and Picro-Sirius Red staining was performed under standard conditions (Applied Medical Research Laboratory, Osaka, Japan). In a histological analysis of murine samples, the degrees of interstitial fibrosis in Sirius Red-stained kidney sections were scored semi-quantitatively with Image J in five random images at 200× magnification, imaged using a Keyence BZ-X800 Microscope described previously.[56,57] Interstitial fibrosis was quantified using the following scores: 0, 0%; 1, 1–10%; 2, 11–25%; 3, 26–50%; 4, 51–75%; and 5, 76–100%.

Separation of tdTomato-positive proximal tubular epithelia using FACS

The separation of tdtomato-positive proximal tubular epithelia using FACS was performed as previously described.[50,58,59] The kidney cortex was minced and a single-cell suspension was generated using research grade Liberase TL (5401020001: Sigma-Aldrich) and 60 units/ml of a DNAse Inhibitor (D5025: Sigma-Aldrich) at 37°C for 30 min. Cells were washed with PBS two times, filtered through 70-μm and 40-μm cell strainers, resuspended in PBS and 2% FBS with 500:1 DAPI (2 mg/mL), and subjected to FACS using SH800 (SONY). Dead cells (DAPI-positive cells) were excluded during FACS. tdTomato-positive and DAPI-negative cells were collected in DMEM and 10% FBS (Gibco).

Culture media (CM) collection

NRK49F and NRK52E were cultured in a 225-cm^2 cell-culture flask at 37°C in a humidified 5% CO_2 and 95% air atmosphere. The culture was maintained in DMEM supplemented with 5% FBS (Invitrogen, Carlsbad, CA). We administered cisplatin or vehicle to NRK52E when the culture reached 50% confluence. After 6 hours, cells were rinsed two times in sterile PBS and the growth medium was replaced with DMEM containing 1% penicillin and streptomycin (Invitrogen) and 5% FBS (Gibco). The culture was then maintained for 24 hours to condition the medium. After 24 hours, the medium was centrifuged at 500 × *g* for 10 min, filtered through a 0.22-μm syringe filter, and conserved at -80°C until used.

Cell proliferation assay

Cells were seeded at densities of 1 × 10^3 cells/well in 96-well plates. After overnight growth, the medium was changed to CM or medium containing CCN1. Twenty-four hours later, the number of viable cells in each well was measured using the Premix WST-1 Cell Proliferation Assay System (Takara Bio, Shiga, Japan) according to the manufacturer's instructions.

Scratch assay

Cells were seeded on a 6-well plate until the culture reached 90-95% confluence. Cells were then treated with mitomycin C (at the concentration and time indicated) to inhibit their proliferation. Artificial scratch gaps (wounds) were made in each cell monolayer using a 1000-μl pipette tip, and cells were immediately washed by PBS two times and replenished with fresh culture media. Digital images of the wounded area were acquired at 0 and 24 hours. 5 random views were chosen along the scratch wound in each well and Free Java-based ImageJ image processing software (Wayne Rasband, National Institutes of Health, Bethesda MD, USA) was used to calculate the cell-migrated area by measuring the wounded area at 0 and 24 hours.

Single cell migration assay

We evaluated individual cell migration using CellDirector 2D (Gradientech, Uppsala, Sweden), which enables analyses of cell migration and cell behavior within chemotactic concentration gradients.[60] Two different cell culture media solutions are used for each CellDirector 2D experiment. CellDirector 2D has three compartments, one with two mediums forming a concentration gradient compartment and one with only each medium compartment. The source medium contains the substance to be evaluated. CellDirector 2D was coated with gelatin solution (Sigma-Aldrich) and placed in an incubator for 30 minutes. Cells were seeded in the chemotaxis chamber, and then treated with mitomycin C (3μg/ml 1hour) to inhibit their proliferation. After 3 hours, a disposable

1 mL syringe was filled with one medium while a second syringe was filled with the other medium. An infusion micro syringe pump (AS ONE Corporation, Osaka, JAPAN) was used to induce flow through the assay at a pump rate of 1 μl/min. Gradients are formed in the centrally positioned gradient region by diffusion of the chemotactic substance between fluid streams generated from the two different media solutions. CellDirector 2D also features two control regions where cells experience no gradient, but instead are exposed to only the source or the sink media solutions. The assay was placed under a live-cell imaging microscope (JULI Stage, NanoEnTek, Seoul, South Korea) in a 37°C incubator room. Digital images were automatically collected every 5 min for up to 16 hours . 5 random views were chosen and migration data from both gradient conditions, as well as from controls, were collected. Tracking data were analyzed using Tracking Tool software (Gradientech). The mean accumulated distance and mean displacement of migrated fibroblasts were analyzed.

RNA extraction and real-time quantitative PCR

Total RNA was extracted from the kidneys, FACS-sorted cells, NRK52E, or NHDF using TRIzol (Life Technologies, Carlsbad, CA) and DirectzolTM RNA MiniPrep (Zymo Research, Irvine, CA) according to the manufacturers' protocols. Complementary DNA was then synthesized using a Prime Script reverse transcription (RT) reagent kit (RR0471A Takara Bio Inc., Shiga, Japan). The real-time detection of PCR products was performed using KAPA SYBR FAST qPCR Master Mix (2×) (KK4602: Kapa Biosystems, Wilmington, MA) and a Thermal Cycler Dice Real Time System (Takara Bio Inc., Shiga, Japan). An initial denaturation step was performed at 95°C for 10 min, followed by 45 cycles of amplification at 95°C for 10 s, 62°C for 10 s, and 72°C for 30 s. The specific primer pairs used for PCR are listed in Table S2.

Western blot analysis

Total cell extracts were obtained using lysing buffer 17 (895943: R&D Systems, Inc., Minneapolis, MN, USA) at room temperature for 5 min. After sonication, proteins were denatured by heating at 95°C for 5 min and separated by SDS-PAGE. Proteins were then transferred onto polyvinylidene difluoride membranes (Immobilon-P IPVH00010: Millipore, MA, USA). After blocking in 5% non-fat milk in TBS/0.1% Tween 20 at room temperature for 1 hour, the membrane was incubated with the corresponding primary antibody (Table S1) at 4°C overnight. After washing with TBS/0.1% Tween 20, secondary antibodies (Table S1) were added. Chemiluminescence was detected using an ECL select Western blot detection reagent (RPN2235: GE Healthcare UK Ltd., Amersham Place, England) or Clarity Max western ECL substrate (1705062: Bio-Rad Laboratories, Inc., Hercules, CA, USA). Signal intensities were evaluated using ImageJ software (National Institutes of Health, Bethesda, MD).

Knockdown by siRNA

The knockdown of Ptk2 was performed as previously described.[52] Duplexed Silencer Select RNA inhibition against protein tyrosine kinase 2 (Ptk2; s130268 and s130267, Invitrogen) and a negative control (no. 4390843, Invitrogen) were transfected using Lipofectamine RNAiMAX reagent (Invitrogen) following the manufacturer's protocols as previously described.[61] Cells were used for assays 48 hours after transfection. siRNA sequences were as follows: Ptk2#1 siRNA sense 5=-GAUGUUGGUUUAAAGCGAU-3= and antisense 5=-AUCGCUUUAAACCAACAUC-3=, Ptk2#2 siRNA sense 5=-GAACAAUGAUGUGAUCGGU-3= and antisense 5=-ACCGAUCA CAUCAUUGUUC-3=.

KO of CCN1 in tubular epithelia by CRISPR-Cas9

The KO of the rat CCN1 gene was performed as described.[62] We used CHOPCHOP (http://chopchop.cbu.uib.no/) according to a previously reported method[63] to design gRNA that targeted exon 2 in the rat CCN1 gene. Bsmb1 linkers were added to gRNA targeting exon 2, CTGCGCGAAGCAACTCAACGAGG (PAM is underlined), and oligos were then annealed following a standard protocol and ligated into the vector, plentiCRISPR v2 (Addgene, plasmid #52961; http://n2t.net/addgene:52961; RRID:Addgene_52961) and confirmed by sequencing. The use of plentiCRISPR v2, which is constructed around a 3rd generation lentiviral backbone, allows for the simultaneous infection/transfection of the vector for the expression of Cas9 and gRNA and selection for puromycin resistance. NRK52E were transfected with a vector (pLentiCRISPR v2) coding for puromycin acetyl-transferase, Cas9, and sgRNA. Twenty-four hours after transfection, puromycin was added to the culture to select transfected cells. Forty-eight hours later, puromycin was removed and cells were allowed to grow for four days. At that time, surviving cells were subjected to cloning by limiting dilutions, a colony from a single cell clone was picked up with cloning rings, and cells were passaged to a 6-well plate as previously described.[64] To confirm the deletion of protein expression, cell lysis and Western blotting were performed using antibodies to CCN1 or GAPDH.

Immunofluorescence analysis

Regarding immunofluorescence, sections were rehydrated and permeabilized with 0.5% Triton X-100 in PBS for 5 min. Samples were blocked with 10% normal goat serum in PBS and sequentially incubated with the primary antibodies shown in Table S1 at 4°C overnight, followed by an incubation with dye-conjugate secondary antibodies (Table S1) at room temperature for 1 hour. Nuclear counterstaining was performed using DAPI or DRAQ5 (DR50050; BioStatus, Leicestershire, UK; 1:2000), followed by mounting in Prolong-Gold (Thermo Fisher Scientific, Waltham, MA). Images were obtained by confocal microscopy (FV1000, Olympus).

Immunohistochemistry analysis

After deparaffinization, sections were placed in citrate-buffered solution (pH 6.0) and boiled for 5 min to retrieve antigens. Endogenous peroxidase was quenched with 3.0% H_2O_2 in methanol for 20 min. Blockade was performed using 3.0% BSA (Nacalai Tesque, Kyoto, Japan) in PBS for 30 min. Sections were then incubated with primary antibodies, as provided in Table S1, followed by an incubation with horseradish peroxidase-conjugated secondary antibodies (Table S1). Diaminobenzidine chromogenic substrate (K3468, Agilent Technologies, Santa Clara, CA) was used for color visualization followed by counterstaining with hematoxylin. All sections were observed using an Eclipse E600 microscope (Nikon, Tokyo, Japan).

RNA sequencing (RNA-seq)

NRK52E were treated with vehicle or 40 μM of cisplatin for 6 h and subsequently cultured with DMEM with 5% FCS for 24 hours. NRK49F were treated for 24 hours with CM from untreated or 40 μM of cisplatin-treated NRK52E. After RNA extraction, RNA samples were provided to the NGS core facility of the Genome Information Research Center at the Research Institute for Microbial Diseases of Osaka University for library construction and sequencing. Library preparation was performed using a TruSeq-stranded mRNA sample prep. kit (Illumina, San Diego, CA) according to the manufacturer's instructions. Sequencing was performed on an Illumina HiSeq 2500 platform in a 100-bp single-end mode. Sequenced reads were mapped to rat reference genome sequences (Rnor6) using STAR v 2.7.10a (https://github.com/alexdobin/STAR/) and uniquely mapped reads were counted by the featureCounts function in the Subread package (https://subread.sourceforge.net).

Bioinformatic analysis

Data analyses were performed using R software version 4.1.2 (https://www.R-project.org/). The edgeR package was used for a differential expression analysis.[65] Genes with FDR < 0.05 and an absolute log2 fold change > 1 were considered to be significant differentially expressed genes. The fgsea package was used for a gene set enrichment analysis. The SCENIC package was employed for a gene regulatory network analysis.

Human *CCN1* expression analysis using published datasets

A preprocessed bulk RNA-seq dataset of the human transplanted kidney (GSE126805) and a single nucleus RNA-seq (snRNAseq) dataset of human healthy and injured kidneys (https://cellxgene.cziscience.com/collections/bcb61471-2a44-4d00-a0af-ff085512674c) were used for the human CCN1 expression analysis.

Seurat v.4.3.0 was employed for a snRNAseq data analysis and visualization. Original cell type annotation was used for a correlation analysis of HAVCR1 and CCN1 expression.

QUANTIFICATION AND STATISTICAL ANALYSIS

Results are expressed as means ± SEM. At least 5 high-power field images for each kidney were used for quantification. Histology was scored by two nephrologists in a blinded manner, and average scores were calculated for all parameters. Statistical analyses were performed by an unpaired *t*-test for comparisons of two variables and by ANOVA and Tukey's post hoc test for comparisons of multiple variables. Pearson's linear correlation coefficient analysis was used to assess the relationship between two quantitative variables. GraphPad Prism was used for all analyses. P values of <0.05 were considered to be significant. Statistical details of each experiment can be found in the figure legends.